Politecnico di Torino

Politecnico di Torino

Corso di Laurea
A.A. 2024/2024
Sessione di Laurea Marzo/Aprile 2025

Numerical investigation of the effect of voids in composite materials

Relatori:
Davide Salvatore Paolino
Alberto Ciampaglia
Carlo Boursier Niutta

Candidati:
Matteo Picus

Summary

1 Abstract

The thesis revolves around the study of the effects of voids on the mechanical properties of a ±45° unidirectional glass fibre reinforced composite.

Voids are a widely studied defect on composite materials, as they are very common and have a significant detrimental effect on the mechanical properties. Also, as their total elimination is a difficult and expensive process, they need to be tolerated and their effects need to be accounted for.

The reduction in mechanical properties, such as Young's modulus and ultimate stresses, is due to the fact that, at the voids tip, a stress intensification phenomenon arises, and facilitates the creation of a crack. The lack of a quantitative analytical characterization in literature of this effect, is due to the statistical variability of the voids shape, size, location and volume fraction, as they all play a non negligeable role in the stress intensification phenomenon. This opens the possibility of a numerical study, based on finite element method. This thesis proposes a procedure for such numerical study.

The procedure is based on a comparison of the real microstructure of a specimen with an ideal one, reconstructed by eliminating all the defects. The microstructure of the real specimen has been reconstructed via a CT scan of the material.

The simulations have been done using the LS-Dyna software. The object of the simulation was a representative volume element (RVE), which is the smallest volume of the composite that is still capable to reproduce the mechanical properties of the whole specimen. To account for the statistical nature of the problem, various RVE's have been subjected to the simulation.

The set up of the simulation, which involves boundary conditions, material properties, type of solver, material failure criteria and more, has been chosen starting from theorical assumptions, empirical data, and widely used methods in finite element simulations of RVE's. By comparing different possibilities and analysing them, a final trade off between accuracy and speed of the solution has been chosen.

The real specimen has been also subjected to a tensile tests, an the results were used to check the correctness of the numerical solution. Once the definitive simulation set up was confirmed, the comparison of various RVE's with the ideal RVE has been done, so that the statistical difference between different types of defects has been taken into consideration.

2 Introduction

Composites are a family of materials characterized by the fact of being made from two chemically different constituents, which, combined together, create a new macroscopic material. The chemical difference is the main factor that defines this class, as the constituents must remain separated, and not merge in a single continuous material. For example, metallic alloys are not considered composites, despite being made from two different elements. Technically, to fit the definition, the constituents could always be mechanically separated.

Examples of composites can also be found in nature; for example, wood is made by cellulose fibres, glued together by lignin.

In the modern world, artificial composites are born with the idea of combining the two different materials, so that the mechanical properties mix and the advantages of both constituents can be exploited.

In composites, three main components are distinguished: the fibres or particulate, the matrix, and the interface. Fibers or particulate are the strongest part of the composite, and have the job of sustaining the load, while the matrix has to transmit the load between fibres, protect them, and hold them in place. The interface conveys the load between the fibres and the matrix. Examples of composites can be seen in figure 1.

Composites can be classified on the basis of the types of constituents, which can be metallic, ceramic, or plastic. The most common are ceramic-plastic composites, where the fibres are made of glass or carbon, and the matrix is a plastic material (usually of the thermoset type).

They are widely used because they guarantee similar mechanical properties compared to steel and aluminium but are much lighter. Lightweightness guarantees better performances and lower fuel consumptions, in applications like aerospace and automotive. They are also widespread in other types of industries such as bio-medics, computers, consumer goods, and a lot more.

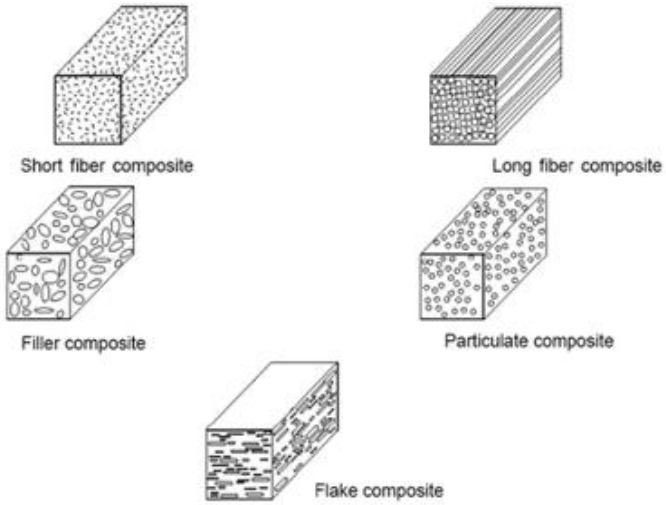

Figure 1 – Scheme of different types of composite materials

Composites are an active field of research, and the topics of interests regard mainly the study and predictability of their mechanical properties. This involves taking into account the possibility of the presence of defects due to the manufacturing process. Defects may arise from a variety of causes, and they have a detrimental effect on mechanical properties, which can not be neglected. This thesis will focus on the study of voids, which are the most common type of defect.

2.1 Voids in composite materials

Voids are the most common type of defect that can be found in composite materials. This is due to various causes, each depending on different phases of the manufacturing process. Usually, the main reason is that air gets trapped inside the matrix, but they can also generate from gases previously dissolved on the epoxy resin, or also chemical reactions that produces these gases.

The main characteristics of voids are their shape, size, location, and the amount. This last characteristic is evaluated referring to the void volume fraction, expressed as a fraction of the void volume over the total volume. This is the most common index, as it is easy to evaluate by means of measuring the volume and weight of the product and the constituents. Other characteristics can be evaluated by other techniques, such as ultrasonic testing, microscopy, or CT scans.

Voids are classified in three different categories, based on their size: macrovoids, mesovoids, and microvoids.

- Macrovoids are the biggest type and can usually be seen with the naked eye. They are mainly due to poor impregnation, where certain parts of the product are bypassed by the global direction of flow of the matrix, but also by a bad layup process that lets air be trapped between laminas.
- Mesovoids are smaller, and they can be found between tows. The driving mechanism for their formation is the bad diffusion process of the matrix during impregnation, described by Darcy's law.
- Microvoids are the smallest type, and they can be found between fibres, inside bundles. In this case, as the space between fibres is very small, the main driving force is the capillary flow, which is the adhesion of the liquid resin to the single fibres.

If the formation of macro voids is usually due to poor process parameters, such as low permeability in some zones, poor resin flow geometries, and can be avoided more easily, micro and meso void formation have contrasting solutions. For example, mesovoids can be avoided by increasing flow velocity and lowering resin viscosity, which increase the hydrodynamic type of flow. On the other hand, microvoids can be avoided by decreasing velocity, and increasing viscosity and surface tension. This is due to the fact that the capillary and hydrodynamic flows have opposite characteristics.

To get the best result, it is necessary to find a good trade-off between micro and meso void formation. For this reason, an index called capillary number has been implemented. The capillary number is equal to:

$$Ca = \frac{\mu V}{\gamma \cos\theta} \tag{1}$$

Where μ is the viscosity, V the velocity of the flow, ϒ is the surface tension and Θ the angle between fibre direction and flow direction. A low capillary number will lead to high concentration of meso voids, and a high value is an index of prevalent micro void

formation. The right trade-off has to be found on a case-to-case basis. A schematic representation of the competition between void formation mechanisms can be seen in Figure 2.

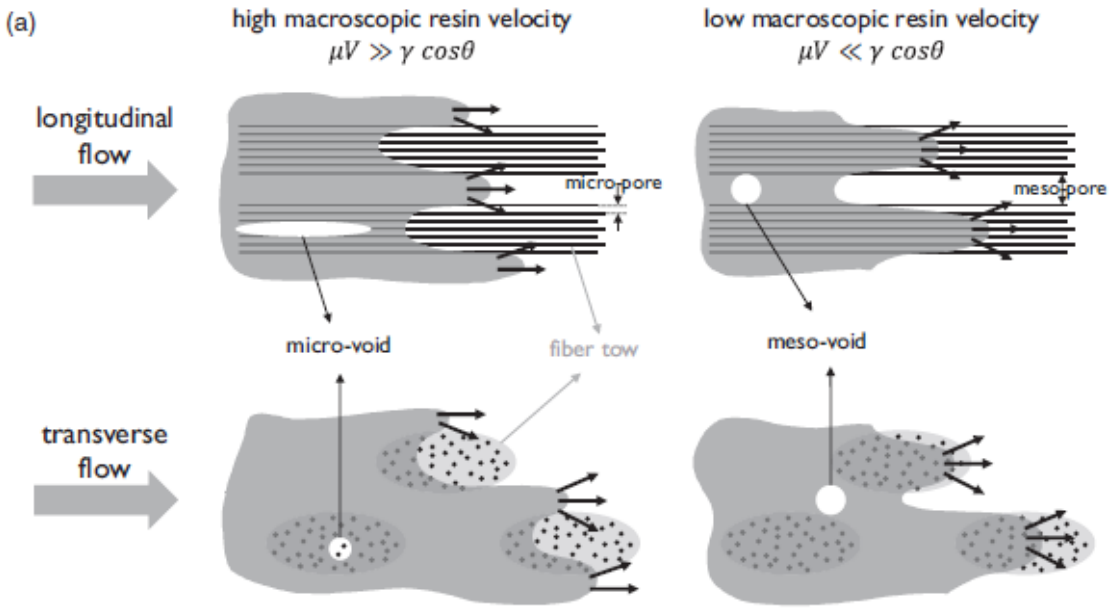

Figure 2 – Schematic representation of micro and meso voids formation

There is also another type of void, which is the intra-laminar void. Usually, the previous types are a main focus in resin transfer moulding (RTM) processes, where the fibres are put in place and the resin is forced to impregnate the space between them. Intra laminar voids are a main topic when pre-pregged fibres are used.

Pre-pregged fibres are common in a lot of fields, due to their commodity and ease of use. They are layers of fibres already wetted in a laboratory in a controlled manner and can be purchased and stored at a controlled temperature. The manufacturing process is reduced only to the lay-up process, where each lamina is stacked up onto a mould, and cured. In this procedure, air pockets can become trapped between laminas.

It is important to know that voids, once they are formed, can migrate, expand, or also contract. An increase of pressure usually leads to compression of the voids, but a pressure gradient can also lead to migration and eventually coalescence of smaller voids into a bigger one. Voids can also disappear, if the solubility of these gases in the matrix is high enough, but also solute gases can coalesce into new voids. Rarely, chemical processes can create gases that coalesce into new voids.

These behaviours can all happen, in various ways, during the curing phase. The manufacturing process of epoxy resin composite needs this phase to let the matrix harden and gain its final mechanical properties. Usually this is done in an autoclave, where optimal values of pressure and temperature can be reached for an adequate amount of time.

In autoclave curing, the high pressure usually helps the reduction of void volume percentage, as it can compress the gases and help them dissolve into the matrix. A correct

process involves the optimization of pressure and temperature profiles over time, in a case-to-case basis.

Due to the fact that the infrastructure for autoclave curing is very expensive, out of autoclave procedures are becoming more common. In this case, to create the difference in pressure, void pumps are used. These significantly limits the magnitude of the pressure differential, which is a main driving factor in lowering void volume percentage.

In this case, the technique used is to guarantee a low viscosity of the matrix during the first phase of the curing process, where pressure is applied. This allows the resin to fill in the microvoids and leave back the meso or macro voids. Then, by applying a high temperature, the resin expands and can easily fill in the mesovoids formed.

This procedure is quite complicated and needs to be optimized in a case-to-case basis and is usually much less effective than autoclave curing.

The difference between autoclave and out of autoclave curing gives the opportunity to underline a very important fact, which is at the basis of the work of this thesis: the total elimination, or at least reduction of void percentage under a negligibility threshold is almost impossible to achieve, and is also very expensive. So, voids are a type of defect which have to be tolerated, and their effects have to be known.

As previously stated, another important characteristic of voids, other than the size, the location, and the amount, is the shape. In this case, as the void formations mechanisms are well understood, the shape of voids are well known. For example, round voids are usually small and created due to trapped air or gas, in inter-bundle zones where the flow is slow. On the other hand, elongated voids are present between fibres in intra-tow zones, and in inter-tow zones with faster matrix flow. Usually, intra-laminar voids have a planar shape, with the smaller dimension aligned with the out of plane direction of the lamina.

2.2 Void effects on mechanical properties

The main effect of voids is a reduction of the mechanical properties of the product. This happens because, around the edge of the defect, a stress intensification phenomenon appears, quite similarly to what happens with a crack or a dent. This lowers the matrix capability of sustaining loads and transferring it to the fibres. The stress intensification usually leads to failure due to crack propagation. Let's now look at what happens for the most important material properties:

- **Tensile properties:** as voids are located inside the epoxy matrix, for unidirectional fibres, the effect on longitudinal ultimate stress is quite negligeable in comparison to transverse tensile properties. For example, the reduction in transverse strength can be as high as 10-20% for each percentual increase in void volume fraction. For non-unidirectional composites, the reduction is still significant and depends on the direction of the fibres and the stacking sequence.
- **Compressive properties:** In this case, even the compression on the longitudinal axis of unidirectional composite shows a significant decrement in resistance. This happens because voids create a lack of support for the fibres, which can lead to

easier buckling. This mechanism propagates fibre by fibre, leading to the buckling of adjacent fibres, and ultimately to the failure of the composites. This reduction in compressive strength can be estimated in a few percent for each 1% in void volume fraction increase, depending on each lamina. A representation of this mechanism can be seen in Figure 3. For the transverse compressive strength, the reduction can be up to 15% for each 1% of void volume fraction.

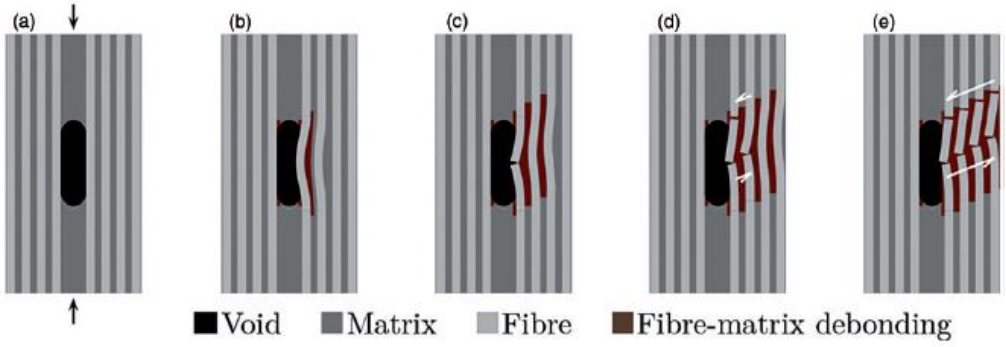

Figure 3 - Damage due to void-assisted buckling under compressive stresses

- **Inter-laminar shear properties:** the presence of inter laminar voids, mainly in pre impregnated composites, affects the inter-laminar shear strength, due to the intensification of stresses around the voids. This reduction can be estimated in 5-10% for each percent increase in void volume fraction. As the other cases, this is very subjective to the geometries, stacking directions, and sequences of each lamina.
- **Shear properties:** as the shear strength of composites is dependent on the matrix properties, it is very sensible to void presence. Even for a low void percentage, the detrimental effect can lead to final strengths that are half, or even a third of the original properties.
- **Fracture toughness and fatigue behaviour** as said before, voids create a stress intensification phenomenon, and this leads to higher stresses around a crack tip, in the vicinities of a void, and ease the process of crack formation. However, this same effect usually slows down the propagation of the crack. As the zones with high stresses are subjected to strain hardening, they slow down the propagation process. Also, when the crack absorbs a void, the void tip becomes the new crack tip, which is less sharp, and leads to lower concentration of stresses.
  This behaviour is the same that leads the fatigue response of composite materials. It explains the fact that, unlike metallic materials, elastic properties decrease quite early in comparison to the failure time of the material, but at the same time, composites are much more damage compliant.
- **Other properties:** there are also other properties that are usually evaluated for composite materials, like impact resistance and flexural resistance, but they are mainly a combination of the previous properties, and in this case the decrement varies a lot on a case-to-case basis.

A very important fact to underline is that this phenomenon is very dependent on the size of the single void, the shape, the location, and the quantity of voids. For example, a void with a blunt end has a lower stress intensification than a void with a sharper end. Also, neighbouring voids can interact with each other, if they are close enough, accelerating or slowing down the process. Also, bigger voids usually lead to bigger stresses than smaller ones. This means that, to know exactly what happens inside the material, it is needed knowing the shape, size, distance, and all the characteristics of all the voids. Given that these are dependent on a lot of parameters of the manufacturing process, and have a high variability, a deterministic approach to the study of the detrimental effect on material properties is almost impossible. This is also showed by the absence of a precise quantitative evaluation of the voids effect in the literature, which is, at maximum, given in approximate percentages, despite the fact that the processes and mechanisms are quite well understood.

Hence, the opportunity of a numerical and statistical approach arises.

3 Procedure

A new approach to the study of the mechanical properties needs the development of a procedure which must be effective, in terms of results close to the real observations, and also time convenient. This proposed strategy will be characterized by computer simulations on the real microstructure of the material, repeated for a statistically significant assessment.

3.1.1 Finite element method

The numerical approach implies the fact that, to get the stress-strain characterization of the problem, the mean used will be a technique based on the approximation of the differential equations into a matrixial multiplication, which can be solved easily by a computer. In this case, the finite element method will be adopted.

Also abbreviated by the acronym "FEM", the finite element method is based on the discretization of the object of the study into small but finite elements. Then, some points on the external surface of that element will be used as nodes, which means that the displacements of these points will be used as variables of the problem. Usually, the nodes are at the vertices of the elements, but this is not necessarily true.

Then, the displacements of a node are linked to the displacements of a general internal point by the linear equation:

$$[u] = [n][s] \tag{2}$$

Where [u] are the displacements of a generic internal point, [s] are the displacements of the nodes, and [n] is a function arbitrarily chosen. Usually, this function is polynomial and its degree depends on the number of nodes. This choice is made because the polynomial is the simplest function that i) guarantees continuity of displacements on the element, ii) allow for rigid body motion, and iii) has continuous first derivative. These conditions are necessary to get to the final formulation of the problem. The higher the number of nodes, the better the precision in the displacement tracking, although at higher computational cost.

Then, by deriving the equation in the spatial coordinates, we get:

$$[\varepsilon] = [b][s] \tag{3}$$

Where [ε] are the deformations, [b] is the derivative of [n], and [s] are the nodal displacements. We can combine this equation with the general elasticity formulation (Hooke's law):

$$[\sigma] = [E][\varepsilon] \tag{4}$$

Which links the stress tensor [σ] with the deformation tensor [ε] via the elasticity matrix [E]. we get:

$$[\sigma] = [E][b][s] \tag{5}$$

Substituting this into the general formulation of the virtual work principle:

$$\int_V [\delta\varepsilon]^T [\sigma]\, dV = \int_V [\delta u]^T [\varphi]\, dV + \int_A [\delta u]^T [\tau]\, dA \tag{6}$$

Which simply states that the internal work is equal to the work made by surface forces and mass forces, the final matrixial formulation can be obtained:

$$[K][s] = [F] \tag{7}$$

Where [K] is the stiffness matrix, [s] are the nodal displacements, and [F] the forces applied to the nodes. The stiffness matrix is calculated as:

$$[K] = \int_V [b]^T [E]\, [b]\, dV \tag{8}$$

And the nodal forces are calculated as:

$$[F] = \int_V [\delta u]^T [\varphi]\, dV + \int_A [\delta u]^T [\tau]\, dA \tag{9}$$

With the same procedure, but using the Lagrange equations, a mass matrix can also be found for the dynamic equation:

$$[M][\ddot{u}] + [K][u] = [F] \tag{10}$$

Once the displacements are known, it is possible to calculate stresses and strains of elements, from the equations (5) and (3).

The finite element method has been widely studied and perfected over the years. It is now possible to use it in non-linear problems, increase the precision with the extra shapes method, decrease the computational weight with under-integrated elements, and so on. Over the years, different FEM commercial softwares were developed. The one that has been used in this study is LS-Dyna™.

3.1.2 Ls-Dyna™

Ls Dyna™ is a commercial software initially developed at the Lawrence Livermore National Laboratory by the United States Government in 1976. This code has been updated and improved during the years and was acquired by *Ansys Software*™ in 2019.

The software is based on the use of keywords, which are commands given by a word preceded by the "*" symbol. This keyword specifies to the software which type of information will follow, and the meaning of the subsequent numbers. For example, the keyword "*MAT" specifies that the following numbers will refer to material properties, and "*SOLID_ORTHO" specifies that an orthotropic solid element is being defined. The software itself is the solver, where commands are given and calculation are made. But, as writing commands directly in keyword language can be difficult, various preprocessing

and postprocessing tools have been developed. These allow to visualize results and the meaning of the commands that are inputted.

For this study, LS-PrePost™ will be used, which is developed by Livermore Software itself.

3.1.3 Statistical approach and representative volume element

As said in the introduction, there is a high dependence of the effect of voids on the mechanical properties on shape, size, amount and location of them. These parameters depend on a variety of mechanisms and variables that can not be controlled and prevent the analytical study of the problem. It is necessary to abandon the particular approach and use a global methodology, where the variability is studied in a statistical way.

The intensification of stresses around voids can lead to very high stress gradients around the tip. This means that, to have a good representation of what happens, the elements must be small enough. Having small elements leads to an exponential increase of the number of nodes, so that simulating the entire composite specimen would lead to a matrixial problem which can not be solved in reasonable times even from very powerful computers. For this reason, it has been necessary to introduce the definition of a representative volume element.

A representative volume element, shortened by the acronym “RVE”, is the smallest volume of material that still retains the macroscopic mechanical properties of the specimen. This volume is found iteratively, by simulating some candidate volumes and measuring the mechanical properties against empirical results of the global material, until a satisfying agreement is achieved. This definition allows to study a smaller volume of material and solves the problem of the size of the stiffness matrix. An example of RVE is presented in Figure 4.

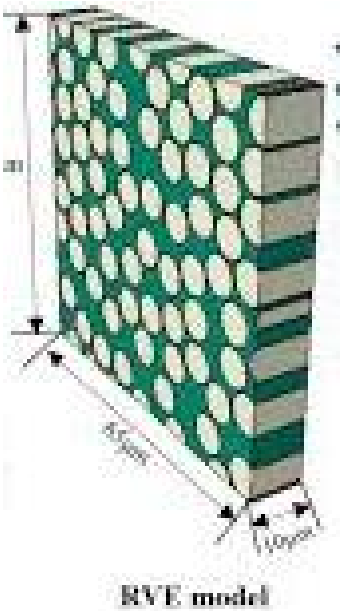

Figure 4 – Example of an RVE of a unidirectional composite

The issue with the standard definition of the RVE is that it is subjected to a local bias. This means that by choosing a certain volume, all the defects and particularities of all the other parts of the material are neglected. This can lead to imprecision in the results, because the particularities of each void, misalignments and other defects have an important impact to the mechanical properties. For this reason, the idea of a statistical volume element (SVE) has been introduced.

A statistical representative volume is not a single volume, but is a stochastically significant number of simulated RVE’s, so that it is possible to have a statistical representation of all the defects of the material. In this case, the mechanical properties are not represented by a single number, but by a statistical distribution, with a mean and a standard deviation. This approach allows to gain a comprehensive understanding of the effect of voids on mechanical properties.

3.1.4 Objective of the study and procedure

The goal of this study is to define a procedure to get a quantitative representation of the effect of voids on mechanical properties of composite materials. This will be done by simulating, with the finite element method, an adequate number of statistical volume elements, and check the results against a perfect RVE, reconstructed from the real material geometry. The SVE's can be studied under a certain amount of in-plane stress cases, and the results will be checked against some failures criteria from literature.

The procedure can be summed up on the following flowchart:

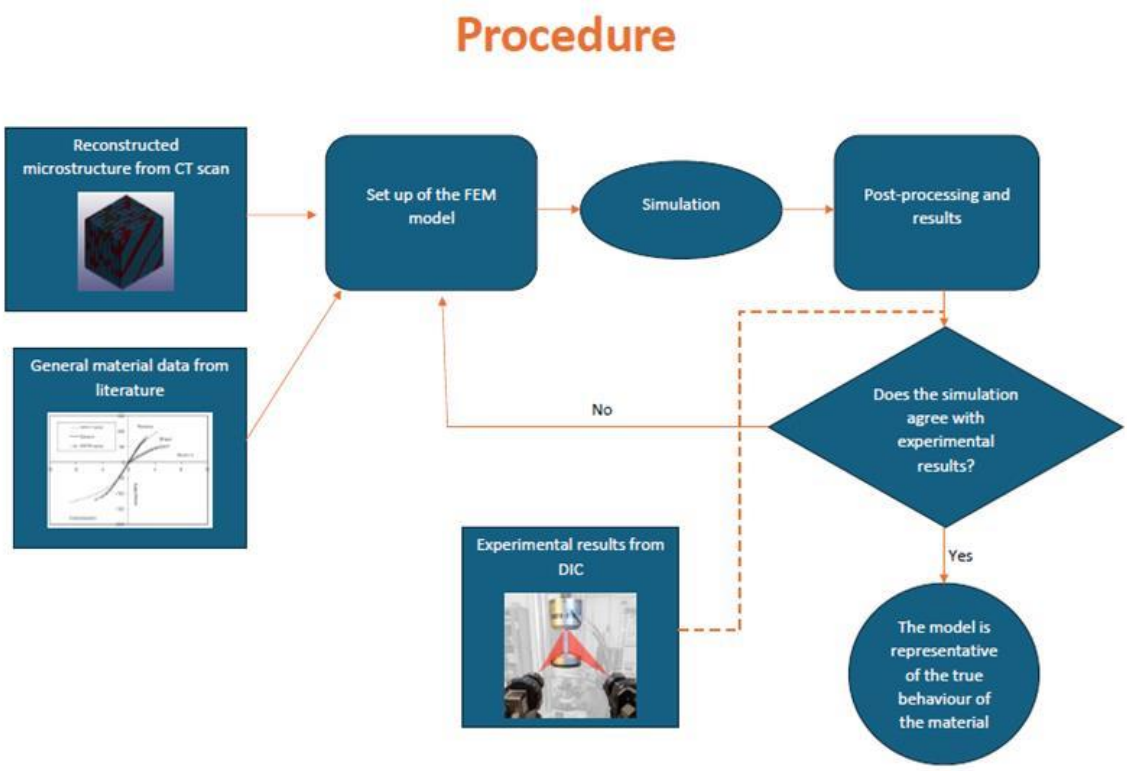

4 Constituents

The material studied will be a glass fibre reinforced composite with an epoxy resin matrix. It is made by twelve layers of unidirectional fibres, stacked in a ±45° sequence. The volume fraction of fibre bundles over the whole volume is approximatively 62%.

The specimen has been already subjected to a tensile test, which will be useful to check the rightfulness of the FEM model. The same material has been also subjected to a CT scan, which allowed to get a tridimensional representation of the microstructure in voxels (tridimensional pixels). The computer tomography resolution is 10 µm. For this reason, it was not possible to capture the single fibres, but only the bundles.

Material properties have been retained from [6], a data sample given in the second world wide failure experiment.

4.1 Matrix modelling

The matrix will be modelled as an isotropic elastic-plastic material. The mechanical properties have been taken by the stress strain curve of an epoxy matrix, which can be seen in Figure 5, with a 24% content of biomaterial [19]. This has been done for two reasons:

- Firstly, mechanical properties data of the bulk resin used in this case was not available, so it was necessary to refer to typical data of general epoxies.
- Secondly, as explained in [15], epoxy resin shows high ductility at a microscale level, and for this reason, general bulk material data proved to be insufficient for describing the real behaviour of the RVE. Data presented in [19] have been obtained through Digital Image Correlation (DIC), thus allowing to accurately

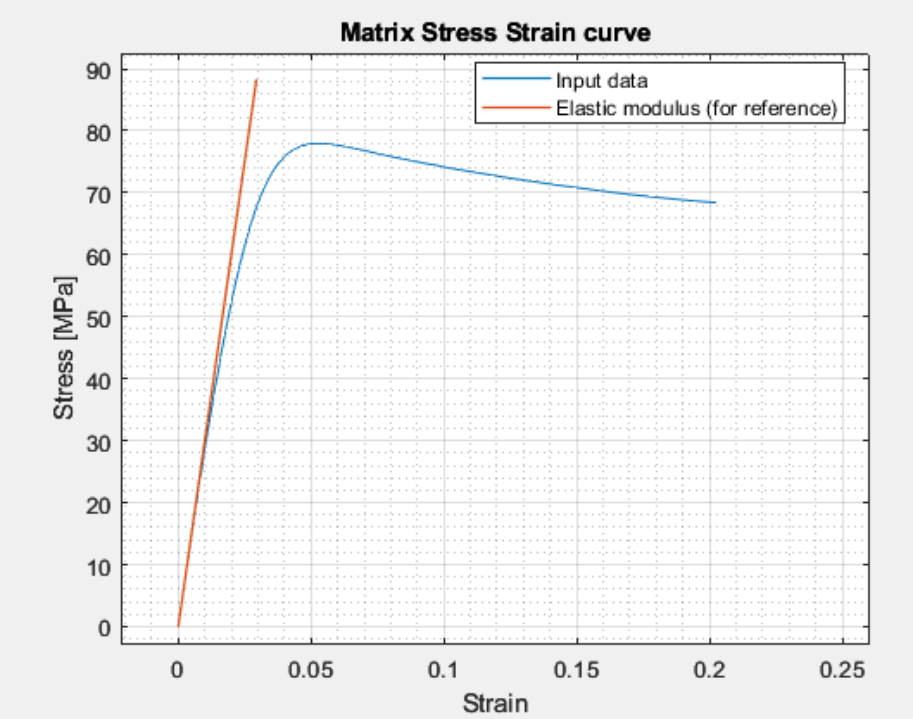

Figure 5 - Matrix stress-strain curve

capture the true stress-true strain response of the material even in the post-peak stage, where necking occurs. The amount of organic material inside the resin has been deemed non-influential on the final properties.

Matrix Properties	
Density [g/cm^3]	1.55
Young's modulus [MPa]	3000
Poisson's ratio	0.35
Yield stress [MPa]	25
Maximum stress [MPa]	78
Ultimate strain [%]	20

Table 1 – summary of the mechanical properties of the matrix

4.2 Bundle modelling

The bundle properties will be modelled as a unidirectional fibrous composite, which is transversely isotropic, i.e., the material is isotropic in the plane perpendicular to the fibres. Material properties are calculated on the basis of the matrix and fibre characteristics, with the rules of mixtures. These rules come from analytical and empirical considerations and allow the prediction of the composite properties from the constituents ones.

As glass is an amorphous material, its fibres are considered as isotropic and elastic.

E-Glass fibres properties	
Elastic modulus [MPa]	73000
Shear elastic modulus [MPa]	30800
Poisson ratio	0.2
Tensile ultimate stress [MPa]	2150
Compressive ultimate stress [MPa]	1450
Density [g/cm^3]	2.5

Table 2 – Summary of E-glass fibre mechanical properties

For the matrix, the same properties of the epoxy resin will be taken. A bundle fibre volume fraction of 70% will be assumed in the calculations:

- **Density:** this property of the composite can be calculated as the sum of the densities of the materials times the volume fraction of each one:
$$\rho_{comp} = \rho_f V_f + \rho_m V_m \quad (11)$$
In this case, it equals to 2.215 g/cm^3.
- **Elastic modulus on longitudinal direction:** This is the Young's modulus on the fibre orientation direction, and it is calculated as:
$$E_l = E_f V_f + \left(1 - V_f\right) E_m \quad (12)$$
which is a weighted sum on the volume fraction. The value obtained is equal to 52000 MPa.

- **Elastic modulus on lateral directions:** In this case, the formula obtained from the theory is similar to the previous one, where the weighted sum is made on the inverse of the elastic moduli of the materials. This formulation has been found to be imprecise, so an empiric correction formulated by Halpin and Tsai is used:

$$\frac{E_t}{E_m} = \frac{1 + \zeta \eta V_f}{1 + \eta V_f} \tag{13}$$

where:

$$\eta = \frac{\frac{E_f}{E_m} - 1}{\frac{E_f}{E_m} + \zeta} \tag{14}$$

The ζ coefficient, which appears in both definitions, depends on the shape of the fibres. In this case, for a round section, it is equal to 2. The value obtained is 4145 MPa.

- **Major Poisson's ratio (ν_{12}):** it is the ratio of deformation in the tangential axis if a force is applied on the longitudinal one. It is calculated as a weighted sum of the Poisson's ratio of fibre and matrix, similarly to the elastic longitudinal modulus:

$$\nu_{12} = \nu_f V_f + \left(1 - V_f\right)\nu_m \tag{15}$$

In this case, the value obtained is 0.245.

- **Minor Poisson's ratio (ν_{21}):** it is the value of ratio of deformation in the longitudinal direction, if a force is applied on the lateral one. The formula in this case is:

$$\frac{\nu_{12}}{E_1} = \frac{\nu_{21}}{E_2} \tag{16}$$

and the value obtained is 0.0195.

- **Shear modulus:** this case is very similar to the transverse elastic modulus one. The theory formulation is not precise enough, the same corrections is used. These similarities are due to the fact that they are both matrix dependent properties, and the redistribution of loads is the same.

$$\frac{G_t}{G_m} = \frac{1 + \zeta \eta V_f}{1 + \eta V_f} \tag{17}$$

where:

$$\eta = \frac{\frac{G_f}{G_m} - 1}{\frac{G_f}{G_m} + \zeta} \tag{18}$$

and η holds the same value. The shear modulus obtained is equal to 1540 MPa.

For the calculation of the limit stresses of the material, it is important to note that tension and compression have different resistance values, as failure depends on the interaction mechanisms between fibres and the matrix.

- **Longitudinal ultimate tensile strength:** In this case, for a 70% fibre volume fraction, the fibres hold most of the load. This is because the displacement is the same for fibres and matrix, but as the first ones are much stiffer, the stresses are

higher. The failure happens when the fibres fail, as the matrix has a much lower ultimate stress, but a stiffness and a volume fraction value that can not generate high enough stresses. The formula for the calculation is:

$$\sigma_{uts,T} = \sigma_f V_f + \left(1 - V_f\right)\tilde{\sigma}_m \tag{19}$$

where $\tilde{\sigma}_m$ is the value of stress reached by the matrix at the ultimate tensile strain of the fibre. The value calculated is equal to 1525 MPa.

- **Longitudinal ultimate compressive strength:** In this case, failure has three possible mechanisms. The first one is represented by a simple failure of the fibres under shear stresses, caused at the 45° angle surface. This happens because under compression or tension, a material has its maximum shear stress in the section at an angle of 45° with the load direction; assuming that the material is perfect, failure happens due to overcoming shear forces on that crystallographic plane. The second one is buckling of the fibres under compressive load and depends on the capability of the matrix of supporting fibres, but also on the fibre geometry (length and section). The third one is the failure of the matrix under tension, caused by the deformation on the transversal axis. If the load is high enough, transversal strain appears due to Poisson's effect and can cause matrix failure.

  To correctly calculate the compressive capacity of the bundle, all three mechanisms should be accounted for and their maximum strength calculated. Then, the minimum strength between all three should be chosen, this procedure is quite complicated and needs information that is not available. To simplify the calculation, the limit will be calculated ignoring the matrix and assuming the first failure mode as the compressive strength of the fibre is given. The limit would be simply 70% of the fibre's compressive strength, equal to 1051 MPa.
- **Lateral and shear strengths:** these cases have the same damage mechanism: due to the fact that fibres are much stiffer than the matrix, they can be assumed to behave like a rigid body. So, in lateral compressive, tensile, and shear cases, all the deformation and the load are taken by the matrix. The presence of fibres inside the matrix acts like a notch, further decreasing the load capacity. To calculate these ultimate strengths, it is suggested to divide the matrix strength values by a notch factor, usually assumed between 2 and 3. In this case, we will use the following empirical formulations, which are more precise:

$$\sigma_{Ttu} = \frac{\sigma_{matrix}}{S_\sigma} \tag{20}$$

$$\tau_{Ttu} = \frac{\tau_{matrix}}{S_\tau} \tag{21}$$

And the scaling factors are expressed as:

$$S_\sigma = \frac{1 - V_f\left(1 - {E_{matrix}}/{E_{fiber}}\right)}{1 - d_s\left(1 - {E_{matrix}}/{E_{fiber}}\right)} \tag{22}$$

$$S_\tau = \frac{1 - V_f\left(1 - {G_{matrix}}/{G_{fiber}}\right)}{1 - d_s\left(1 - {G_{matrix}}/{G_{fiber}}\right)} \tag{23}$$

Where:

$$d_s = \sqrt{\frac{4V_f}{\pi}} \tag{24}$$

The final values are 22.2 MPa for the lateral ultimate tensile stress and 14.94 MPa for the shear ultimate stress.

In the following table, all the properties for the bundle are summed up:

Bundle Properties	
Longitudinal Young's modulus [MPa]	52000
Transversal Young's modulus [MPa]	4145
Main Poisson's ratio	0.245
Transversal Poison's ratio	0.0195
Density [g/cm^3]	2.215
Shear elastic modulus longitudinal direction [MPa]	1540
Shear elastic modulus transversal direction [MPa]	1537
Longitudinal ultimate tensile stress [MPa]	1525
Longitudinal ultimate compressive stress [MPa]	1051
Transversal ultimate tensile stress [MPa]	22.2
Transversal ultimate compressive stress [MPa]	22.2
Shear ultimate stress, longitudinal and transverse direction [MPa]	14.94

Table 3 – Summary of the mechanical properties of the bundle

4.3 One element tests and material cards

A one element test is a simulation done on a single element to check if the chosen material card is coherent with the properties of the real material, and to understand the element behaviour in the simulation. Usually, it consists in a tensile test and/or a shear test, where parameters like ultimate tensile strength, Young's modulus and fracture energy are compared to the goal values.

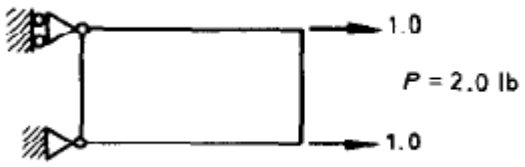

Figure 6 - Example of constraints in a one element test

It is important that the element type is the same as the one used in the main simulation, as some parameters like under-integration can influence the stiffness. The boundary conditions must ensure the unidirectional stress condition. This was achieved by constraining all three displacements at one node of a face, only one displacement at the other points of the same face, and then applying displacements at the opposite face

nodes. Example of constraints in a two dimensional one element test can be seen in Figure 6.

It is important that the material card, the data, and the element type have to be the same of the main simulation. In some cases, where certain material cards perform element size regularization of the data (for example fracture toughness), even the size has to be the same.

For the matrix, the first material card chosen was the 024 (*MAT_PIECEWISE_LINEAR_PLASTICITY). This is a commonly used card, which allows the modelling of elasticity up until a yield point, and then model plasticity with a curve of stress and plastic strain points. The card works adding the plastic strain to the elastic ones. Failure is specified by giving an ultimate plastic strain value, which is used to interpolate a maximum stress for the Von Mises criterion. In implicit analyses, the post-failure behaviour of this card is characterized by a gradual softening of the material, to ensure stability and convergence of the simulation. In explicit analyses, the softening is not present, and the stress and strain values are brought to zero abruptly. To specify the post failure damage, the material card 081 (*MAT_PLASTICITY_WHIT_DAMAGE) can be used. It is identical to the 024, but the ultimate plastic strain triggers damage initiation, and final rupture is specified by another plastic strain value. The default damage model is linear, but a nonlinear one can be specified by a curve. These material cards also allow to account for strain-rate effects, but this was not needed for quasi-static simulations. The damage behaviour of the card 081 is the same in both explicit and implicit simulations.

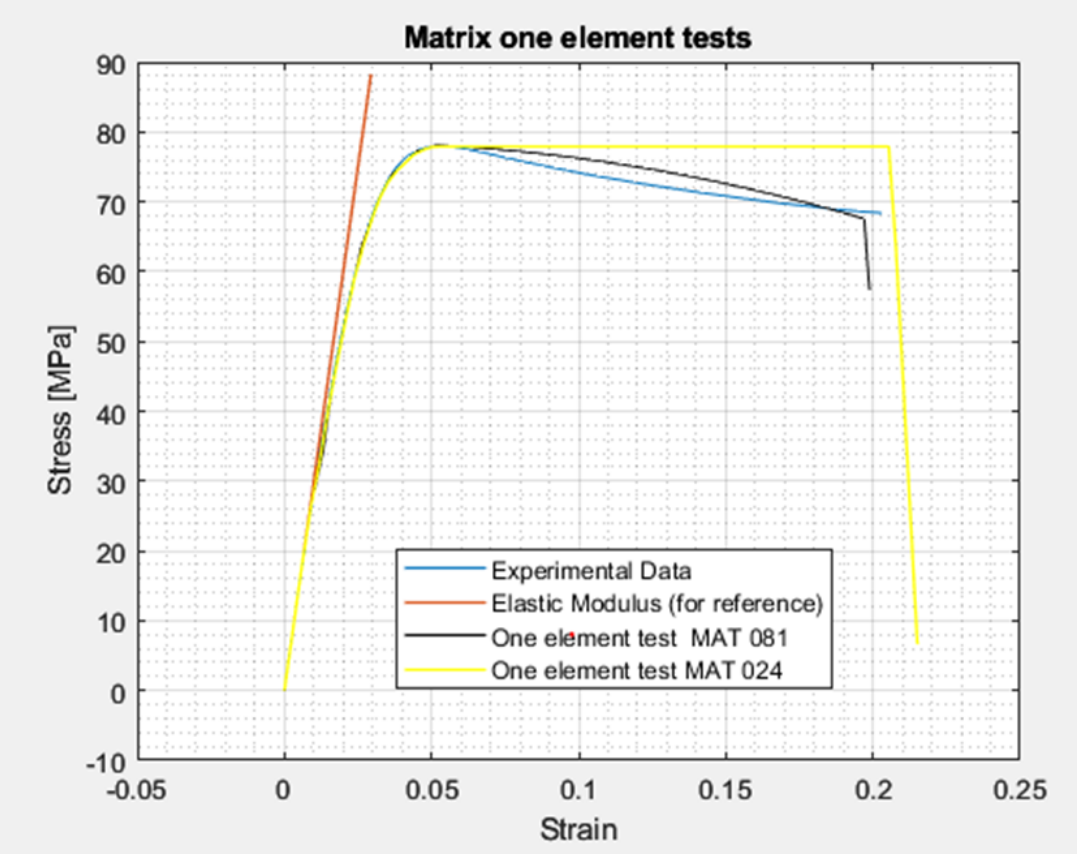

Figure 7 - Results of the single element test against the true points with MAT_081

It was noted that the material card 081 caused numerical instability and bad convergence. This happened when some elements reached damage values close to unity, which means that the elastic properties are close to zero. In these cases, the calculation of the exact damage progression is difficult, especially if nearby elements are also damaged. This does not happen with the card 024, as the damage evolution is not calculated by the software, but the stress is simply brought to zero in a certain amount of steps. Figure 7 shows the comparison between experimental data and the results of the one element tests of the material cards. A more comprehensive review of the behaviour of the cards, and how to fit the models with the empirical curve can be found in appendix B.

For the tows, there are various material cards that allow to model composites, with different failure criterions.

The card 059 (SOLID_COMPOSITE_FAILURE_SOLID_MODEL) is a commonly used material card to model failure in laminated composite materials. The material is treated as linear elastic up until the failure criterion is satisfied. After this point, in implicit analyses, a softening behaviour similar to the one discussed in MAT 024 is present, for stability reasons. That is not the case for the explicit solver, where the stresses and strains are suddenly brought to zero.

The failure criteria for solids is made up of eight smaller criteria: five are linked to shear and tensile stresses, three are linked to compression but are not of interest in this study. The five failure criteria accounted here are:

- Longitudinal tension:

$$\left(\frac{\sigma_{11}}{X_t}\right)^2 + \left(\frac{\sigma_{12}}{S_c}\right)^2 + \left(\frac{\sigma_{13}}{S_c}\right)^2 = f_1 \tag{25}$$

- Transverse tension:

$$\left(\frac{\sigma_{22}}{Y_t}\right)^2 + \left(\frac{\sigma_{12}}{S_c}\right)^2 + \left(\frac{\sigma_{23}}{S_c}\right)^2 = f_2 \tag{26}$$

- Through-thickness shear with longitudinal tension:

$$\left(\frac{\sigma_{11}}{X_t}\right)^2 + \left(\frac{\sigma_{13}}{S_c}\right)^2 = f_3 \tag{27}$$

- Delamination:

$$\left(\frac{\sigma_{33}}{Y_t}\right)^2 + \left(\frac{\sigma_{22}}{S_c}\right)^2 + \left(\frac{\sigma_{13}}{S_c}\right)^2 = f_4 \tag{28}$$

- Through thickness shear with transversal tension:

$$\left(\frac{\sigma_{22}}{Y_t}\right)^2 + \left(\frac{\sigma_{23}}{S_c}\right)^2 = f_5 \tag{29}$$

Where:

- σ_{ab} is the component of the stress matrix;
- X_t is the ultimate strength in the longitudinal direction, in tension, equal to 1525 MPa;
- Y_t is the ultimate strength in the lateral direction, in tension, equal to 22.2 MPa;
- S_c is the shear ultimate failure limit, equal to 14.94 MPa;
- F_n is the failure flag, which indicates that the n^{th} failure has been reached.

Once a failure mode was triggered, the card reduces the stresses linked to such failure modes, and the element is deleted only when σ_{11}, σ_{22}, and σ_{33} are zero.

These failure criteria were not suitable for the modelling of the tow, mainly because of the delamination, which is not a failure mode present in the bundle, as it is not a laminate. Simulations done with this card were unsuccessful, as the delamination failure mode was triggered before all others, and, as the stresses were scaled towards zero, other failure modes were initiated. This resulted in a cascade failure where all the criterions were satisfied, and the element deleted. The final result was a sudden failure of all fibres in the model, which is not a realistic behaviour. For this reason, this card has been discarded.

Another card that has been evaluated is the 054/055 (*MAT_ENHANCED_COMPOSITE_DAMAGE). This material card models the material as linear elastic up until failure. After failure, the stresses are brought down by a factor that can be specified. If for example, the factor is equal to one, the material shows a perfect plasticity. This is very helpful in modelling post failure behaviour in crash simulation.

As regards the failure criteria, it is made up by different criteria:

- Longitudinal fibre failure in tension:
$$\left(\frac{\sigma_{11}}{X_t}\right)^2 + \beta\left(\frac{\sigma_{12}}{S_c}\right)^2 = f_1 \tag{30}$$
if f_1 is greater than one, failure is detected and all elastic components are brought to zero. Beta is the shear factor, which can be modified between zero and one. A factor alpha is also present, which takes into consideration a second order shear stress value, but it is advised to ignore this factor.
- Longitudinal fibre failure in compression:
$$\left(\frac{\sigma_{11}}{X_c}\right)^2 = f_2 \tag{31}$$
if f_2 is greater than one, failure is detected and E_1, ν_{12}, ν_{21} are brought to zero.
- Lateral matrix failure in tension: in this case, if the Chang-Chang criterion is chosen (card 054), the failure of the matrix happens when:
$$\left(\frac{\sigma_{22}}{Y_t}\right)^2 + \left(\frac{\sigma_{12}}{S_c}\right) = f_3 \tag{32}$$
and f_3 reaches one. In this case, E_2, G_{12}, ν_{21} are brought to zero.
- Lateral matrix failure in compression: for the Chang-Chang criterion, the failure is driven by:

$$\left(\frac{\sigma_{11}}{2S_C}\right)^2 + \left[\left(\frac{Y_c}{2S_C}\right)^2 - 1\right]\left(\frac{\sigma_{22}}{Y_c}\right) + \left(\frac{\sigma_{12}}{S_c}\right)^2 = f_4 \quad (33)$$

If f_4 reaches one, E_2, G_{12}, ν_{21} and ν_{12} are brought to zero.

- If the option 055 is chosen, the two matrix failure criterions are substituted by the Tsai-Wu criteria, both in compression and tension. Failure still happens when the flag reaches one, and in this case all material properties are brough to zero.

$$\frac{{\sigma_{22}}^2}{Y_c Y_t} + \left(\frac{\sigma_{12}}{S_c}\right)^2 + \frac{(Y_c - Y_t)\sigma_{22}}{Y_c Y_t} = f_3 \quad (34)$$

These criterions are reported for a biaxial state of tension. In case of a triaxial state, the stresses σ_{33} and σ_{13} are added to the criteria and treated like σ_{22} and σ_{12}. This can also be specified via the transversely isotropic option.

For the out of plane shear properties G_{23} and G_{31}, a strain-based criterion is used. The effective plastic strain, calculated as:

$$\varepsilon_{eff} = \sqrt{\varepsilon_{23}^2 + \varepsilon_{32}^2} \quad (35)$$

Once this effective strain reaches a specified value, degradation of the elastic properties begins. The maximum damage and final strain can be specified.

In the case of explicit simulations, a parameter called “NCYC” can be specified. This spreads the reduction of stresses after failure on a customizable number of steps, which smoothens the drop.

For our purposes, the material 054 has been chosen as the definitive card.

Another material card investigated was the 058 (*MAT_LAMINATED_COMPOSITE_FABRIC), which implements three different failure criterions based on Hashin’s theory. Depending on the “FS” option, which can be seen in Figure 8:

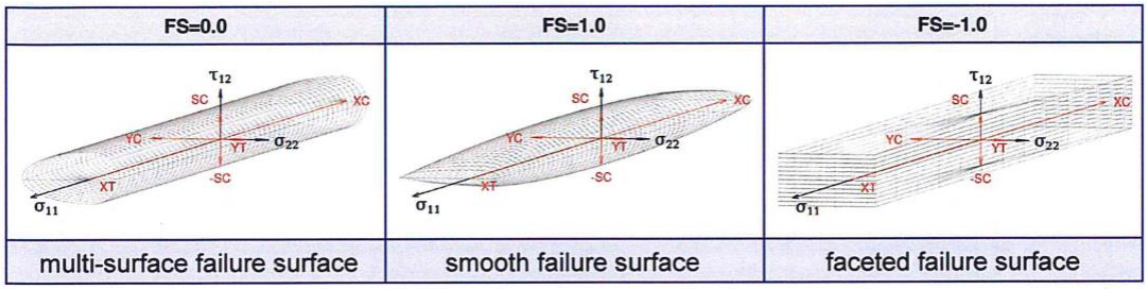

Figure 8 – Visualization of failure criterions for the material card 058

The suggested one for unidirectional fabric was the smooth failure surface one. The main upgrade is that a smooth damage evolution is possible, specifying a minimum stress threshold after failure. Unfortunately, this card was available only for explicit simulations, and required a high number of material parameters, which were not known. For this reason, this card was not considered.

Another material card commonly used is the MAT_022 (MAT_COMPOSITE_DAMAGE). It is the simplest model, which requires the least amount of input data (only elastic properties and maximum stresses must be specified). The failure criteria are the same as the card 054, but with two differences: the beta factor is equal to one by default and can not be changed; the failure in compression for fibres is not present. This card was not considered due to its simplicity, as it did not allow for the necessary customization of the failure criteria and material behaviours.

4.3.1 Void modelling

The modelling of the absence of material is not trivial. The first option would be to directly cancel the elements linked to voids, so that the stiffness matrix has less degrees of freedom and ease the work of the solver. This creates a problem with the periodic boundary conditions, which need the presence of two nodes in the same position of opposite faces. The deletion of elements for representing voids creates absence of material, and accordingly of nodes. If this occurs in the external faces of the RVE, the correct application of periodic boundary conditions is prevented.

Another solution available in Ls-Dyna™ was the material card 09 (*MAT_NULL). This keyword allows the modelling of gases, by only calculating the diagonal elements of the stiffness matrix. This card also needs to be referenced to an equation of state (*EOS keyword). This would also ease the computational cost of the simulation, while still retaining continuity in the boundary faces. In this case, another problem with the same conditions emerged: the null element resulted too loose, and the deformation imposed by the constraint equation would be applied only to the nodes of such element.

The last solution consisted in the modelling of the void as an elastic material with a low young's modulus. This solved the problems with the boundary conditions, but the computation of the stiffness matrix of these elements had to be done. As the void's content is not very high, this cost has been deemed acceptable.

4.4 RVE

Once the material has been chosen and their properties calculated, it is necessary to get the information about the real microstructure of the composite, which means reconstructing the real RVE. This has been done via a computerized tomography (CT) scan.

This procedure exploits the difference in attenuation of x rays in different constituents. It works by sending electromagnetic waves through the material, and thanks to receptors at the other end, it is possible to measure the attenuation of the signal. This gives a bidimensional image in a grey scale of the section of the object; to have a tridimensional representation, the device rotates around the specimen. In this case, 1600 images of the composite were taken, and the results was given as a scale of greys of 256 values. Once the images were obtained, each value of the grey scale had to be associated with either voids, bundle, or matrix. Depending on the value of the scale, a void probability and tow probability factors were assigned to each voxel. They indicate

the probability that each voxel represents either a tow or a void. Then, each one was labelled as bundle if the tow probability was higher than 50% and labelled as void if its factor was greater than 50%.

Another important characteristic of the RVE is its size. In this case, the work has been already done in [5]. The procedure involved the same statistical approach that has been described earlier. Some candidate sizes were considered, and for each size some randomly chosen RVEs were subjected to a tensile simulation in the elastic field. Each test was used to evaluate a mean value and a standard deviation for the transversal Young's modulus, until convergence was reached.

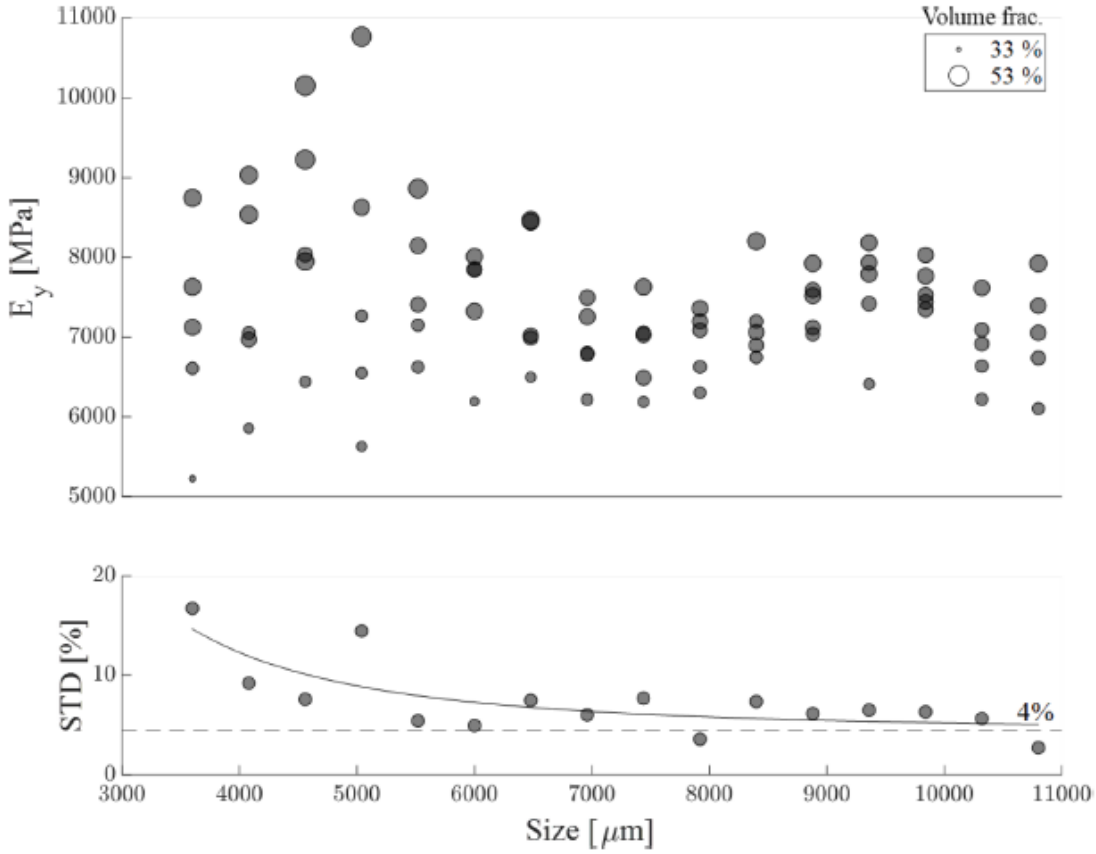

Figure 9 - Convergence procedure results

The RVE is chosen to be cubic, at least until the out of plane dimension reaches a value of 5.5 mm. This is done because that value comprised the 10 middle layers, and the two external ones were unusable due to poor tomography results.

As we can see from Figure 9, a certain amount of internal variation of the specimen is always present. An asymptote for the standard deviation was reached, and it corresponds to a value of 4%. The size chosen is 6.1 mm, as a standard deviation of 5% is assumed acceptable. So, the RVE size will be a 5.5x6.1x6.1 mm.

For the perfect RVE, necessary to make the comparison, a reconstruction was made using TexGen™ software. This is an open-source software that allows creating textile models. To reconstruct the pristine model, some evaluations were made on the real RVE:

- To recreate accurate tow dimensions, some evaluations were made about the cross sections. It was decided to fit the section with an ellipsoidal shape, of which the major and minor axis were determined by a statistical analysis of the bundles in the surface of the RVE. Then, the mean values were taken:
- To accurately represent the spatial layout of the fibres, a visual evaluation was made. It was noted that 10 bundle layers were present, and that each layer had 5 bundles intersecting the volumes.
- The last parameter was the bundle volume fraction. After calculating the real value, equal to 62%, it was used as a benchmark for the ideal RVE value. In the end, the reconstructed RVE had a tow volume fraction of 64%. Considering the fact that the ideal volume does not have voids, this value is deemed acceptable.

An example of extracted RVE and the Ideal one can be seen in Figures 10 and 11, respectively

	Major axis	*Minor axis*
Number of measurements	14	7
Mean value [mm]	1.838	0.5857
Standard deviation [%]	13.23	11.78

Table 4 – Summary of the measurements done in the real RVE

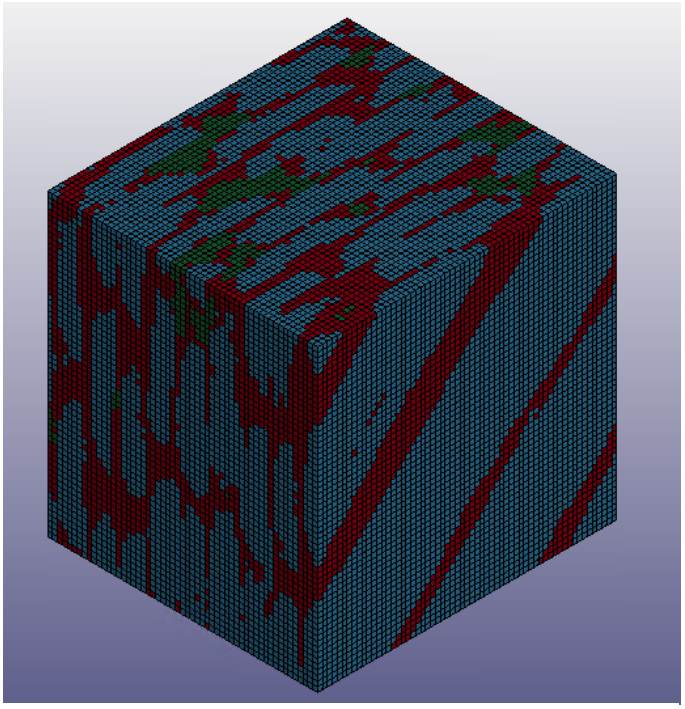

Figure 10 - Image of an RVE. The matrix is coloured in red, the fibres in light blue, the voids in green.

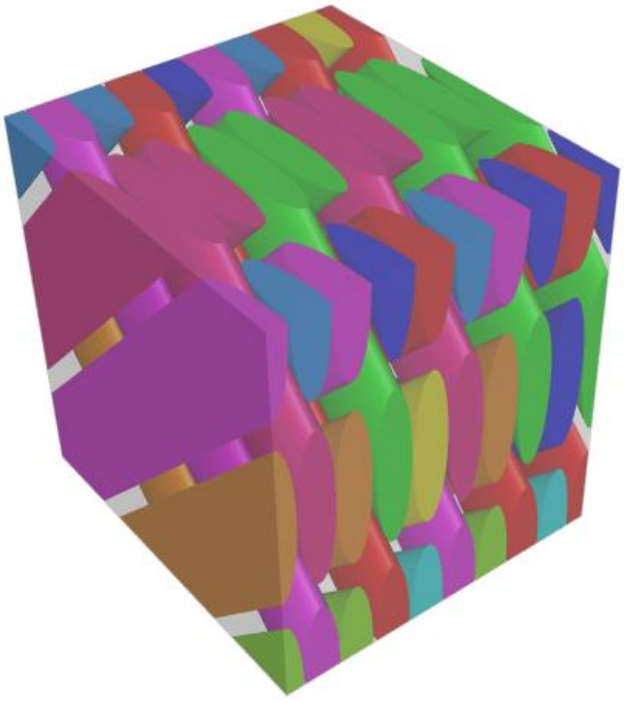

Figure 11 - Image of the reconstructed ideal RVE

5 Methods

Numerical multiscale simulations based on finite element method are an advanced way to estimate the stress-strain state in cases where theorical formulations are not available. This method has been perfected over the years and integrated with other variations and techniques. Achieving a correct solution implies the consideration and optimization of all such parameters, like mesh, elements, boundary conditions, and solution methods.

5.1 Mesh and elements

A correct meshing and choice of elements is very important to have a coherent solution. Elements shape, size, and characteristic such as integrations and number of nodes strongly affect the results. Typically, a trade off between the precision and speed must be found.

In this case, 8 node cubic elements were chosen. This is due to the fact that the output of the CT scan is given in voxels, which are cubic pixels. This made convenient the conversion into a cubic mesh, compatible with the software (Abaqus™ first and then LS Dyna™). This has been possible thanks to the MATLAB™ code [13], which has been adapted for this specific case. An example of 8 node cubic element can be seen in Figure 12.

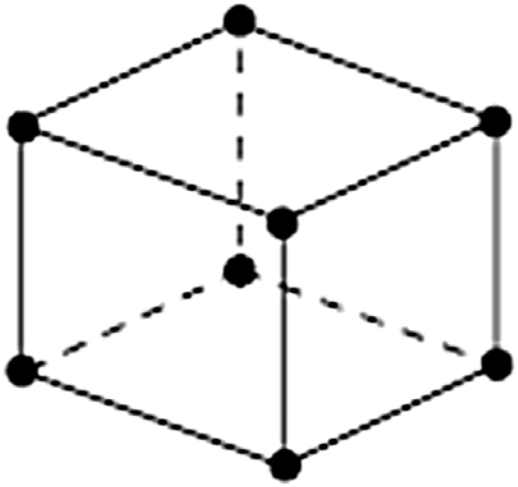

Figure 12 - 8 node cubic element

In the basic 8 node element, the displacements of the nodes are used to interpolate the displacement of a generic internal point of the element. Each node tracks the 3 displacements on x, y, and z direction. This means, that for each direction, the interpolation polynomial of the cube is:

$$n_1 = a_0 + a_1 x + a_2 y + a_3 z + a_4 x^2 + a_5 y^2 + a_6 z^2 + a_7 xy \qquad (36)$$

with 8 constants that can be calculated from the 8 displacements of the nodes. As seen before, the stress vector is described by the derivative of n, called b. If n is a 2nd order polynomial, b is necessarily a linear function.

Another thing that characterizes elements is the integration. As seen before, the stiffness matrix of an element is calculated by:

$$[K] = \int_V [b]^T [E]\,[b]\, dV \qquad (37)$$

The integral of Equation 1 is numerically calculated used a weighted integration scheme:

$$[K] = \sum_{i=1}^{n}\sum_{j=1}^{m}\sum_{k=1}^{l} \xi_i \eta_j \beta_k [b]^t [E][b] \Delta x \Delta y \Delta z \tag{38}$$

Depending on the number of the points where the sum is calculated, and consequently the function b is evaluated, the stiffness matrix could be underestimated. This phenomenon is called underintegration.

Underintegration is not necessarily a problem, but it can also be an advantage. Firstly, under-evaluating the stiffness matrix balances out the fact that the polynomial can not interpolate all the possible displacements of the internal points, which means that the element is inherently stiffer than reality. It also reduces the computational cost of the simulation. Under integration can also depend on the method of calculation of the value of the function on the points: for example, Newton-Cotes algorithm is less precise than Gauss-Legendre one. Excessive underintegration can also lead to problems, such as the hourglass effect.

The hourglass effect happens when an element deforms without an increase in stress or strain values at the integration points. If the underintegration is excessive, the stiffness matrix can be so underestimated that the elements have possible strain modes that presents no stiffness. This means that, despite the movement of the external points, the element does not change its stress and strain values and deforms without opposing any resistance. This effect is called hourglass because cubic and underintegrated elements usually show an hourglass shape when this effect happens. To counteract this phenomenon, softwares developed various techniques, useful to reduce this effect, while still retaining the computational advantages.

Ls Dyna has mainly four types of solid elements: types “1”, “2”, “-1” and “-2”.

- Type “1” is the simplest, underintegrated with only one integration point. For this reason, it can display a constant stress field. This means that it is not very precise and is often affected by the hourglass phenomenon. Hourglass stabilization methods have to be used in this case. The main advantage is that it shortens significantly the simulation time, and it is stable in severe deformation cases, while still being accurate in most applications.
- Type “2” is a selectively underintegrated element, which means that the underintegration is less severe, with 8 integration points purposefully chosen to retain the best performance. The strain field is in this case linear, but the element is slower than the “1”, more unstable at severe deformation, and too stiff for many situations. It can also be affected by shear locking, which is a phenomenon where an element subjected to pure bending has the integration points distributed in such a way that the element cannot bend, but show a shear deformation, which is not correct. To solve this problem, the element choice has to fell on the single integration point element, or if needed, retain the integration points but correct this effect.

- Element types “-1” and “-2” are similar to element type “2” but have the shear locking correction. The two differ for the type of such correction; the first one is more efficient and faster, while the second one has a more accurate formulation.

The difference in speed between material formulations depends on the fact that the material routine takes more time to complete if the integration points are more than one, as the stresses and strains have to be calculated for each integration point. This effect is very noticeable in the explicit solver, as the time steps are much more at the material routine activates at the end of each one. On the opposite, implicit solvers are not affected by this behaviour, but the convergence benefits from having a better interpolation of the stresses inside the element, which means having element types such as -1 and -2. A comparison between simulation times for explicit simulations can be seen in Figure 13. For the cubic RVE, a total of 204655 elements and 215164 nodes were defined.

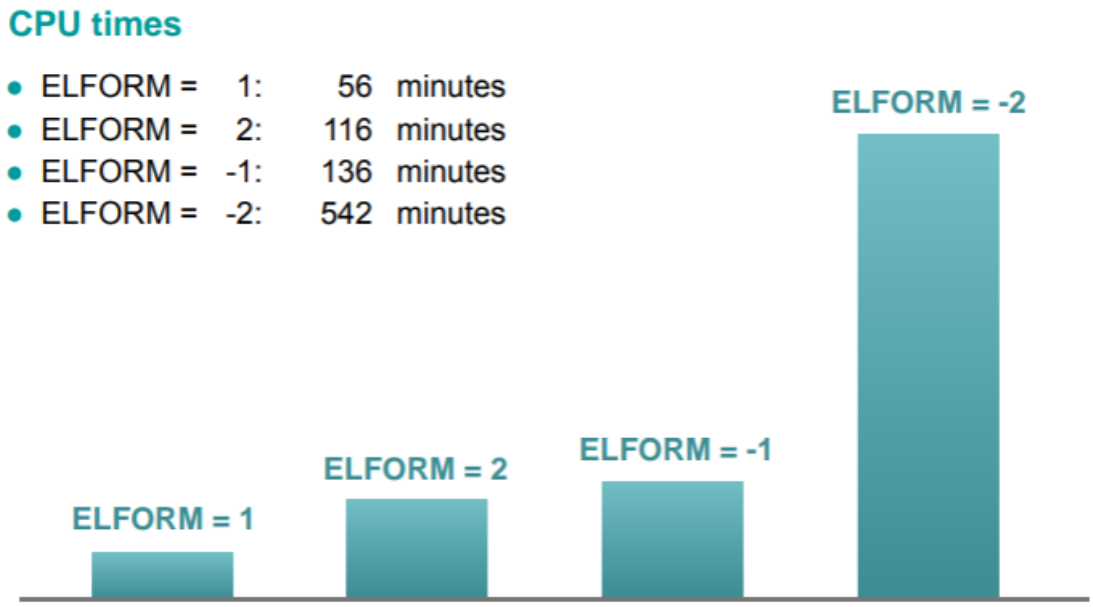

Figure 13 - Comparison of CPU times between different element formulations

5.2 Boundary conditions

The correct application of loads and constraints is important to achieve the correct result, especially when simulating RVEs, where the boundary conditions should replicate a far field strain state $\bar{\varepsilon}$. This is commonly achieved by applying Dirichlet typer boundary conditions on the domain Γ_D.

The simplest way to apply boundary conditions in a uniaxial load case, will be to constrain the movement in all three directions of a face, and apply a load or displacement to the opposite one. In addition, the lateral faces could be constrained to the transversal movement, to account for the presence of material at the sides of the RVE. This approach is called linear kinematic boundary conditions.

$$u_i = \bar{\varepsilon}_{ij} x_j, \qquad with\ x \in \Gamma_D \tag{39}$$

Another approach, which allows to fully simulate the displacements of the RVE inside a material continuum, is the periodic boundary conditions (PBC). The idea is to simulate the presence of material outside the domain by assuming that the continuum is populated by identical RVE's. So, for a generic point in a face, the displacements have to be identical to the one of the point on the opposite side of the RVE.

The first approach is simpler and easier to implement in FEM softwares but has its drawbacks. The convergence previously discussed is reached for higher RVE sizes, as the PBC approach is more realistic.

For the periodic boundary conditions, the constraints linking the nodes are equations: for a certain direction, there are two faces with that direction as normal. For each point in a face, a corresponding point on the opposite face can be found. The condition is that these points have the same displacements, less of a constant. That constant is the global displacement of the material, and it is imposed via a dummy node. For example, assuming that 300 and 500 are the opposing nodes, one of the equations will be the following:

$$u_1^{300} - u_1^{500} = u_1^{dummy} \tag{40}$$

linking the displacement on the direction 1. For each couple of points, there are three equations, for displacements in the x, y, and z directions. If the dummy nodes displacement is set equal to zero, the equation becomes:

$$u_1^{300} = u_1^{500} \tag{41}$$

which states that the displacements have to be identical.

The dummy nodes are three, one for each couple of opposing faces. Their position is not important. For example, to apply a unidirectional stress condition in the x direction, the dummy displacements will be:

- For the x dummy node, the x displacement would be equal to the length of the RVE times the global deformation that must be imposed, while y and z displacements are set to zero.
- For the y dummy node, x and z displacements are set to zero. The y direction can be left unconstrained, to let the RVE freely shrink. Another option is to impose a set displacement equal to the global shrinkage, due to Poisson's effect.
- Similarly to the y dummy node, the z dummy node displacements are set to zero in the x and y directions, and the z direction could be left free or constrained to a global movement.

The nine displacements can be prescribed so that various types of tests can be simulated on the RVE. Adequate care has to be taken for the vertices and edges, as they are nodes that belong to two or three faces simultaneously. Further explanation of how to impose constraints in these cases is given in [12].

The main difficulty is that these equations have to be written externally and then imported. As the number of nodes is quite high, it is necessary to develop a code that

automatically writes all the constraints. For this case, a MATLAB™ code was already available at the DIMEAS department and needed only some adaptations for the syntax. In total, 31827 equations were written. In LS-Dyna, the keyword which allowed to import the equation is *CONSTRAINED_MULTIPLE_GLOBAL.

Periodic boundary conditions have been proved to have a main drawback in explicit simulations. As specified in the Ls-Dyna manual, in explicit analysis only one constraint type can be specified to a node or rigid body. As the dummy node needs more than one constraint type, to be subjected to a controlled displacement with the *PRESCRIBED_MOTION_NODE card, Ls Dyna solves the conflict ignoring the last one, and the simulation does not show any movement. An attempt to simulate a rigid body, applying the displacement to a node linked via an elastic element to the dummy nodes, results in numerical vibrations that erode elements. Similar problems were found in [8]. For this reason, the explicit solver will be used with linear kinematic boundary conditions.

Another characteristic of Ls Dyna is that, to optimize the calculation, it eliminates the nodes that are not referenced to any element. This happens at the first deletion of an element, and it is done because an unreferenced node is supposed to be what remains of the erosion of surrounding elements, and does not have any remaining functions. This also led to the deletion of the dummy node in the middle of the simulation. To prevent this, dummy elements were created. They are elements which only purpose is to be a reference to the dummy node, so that this erosion procedure is not triggered. They can be treated either as a rigid element, or a very soft material, which nodes have to be constrained so that the element moves as a rigid body. This last solution was implemented with the keyword *CONSTRAINED_MULTIPLE_GLOBAL, which imposed equal displacements of the dummy node and another node of the dummy element.

Another effect of the choice of the boundary conditions is the change in simulation time, mainly for implicit simulations. The building and inversion of the stiffness matrix is influenced by the boundary conditions in a substantial way; it has been observed that, with linear kinematic conditions, the matrix inversion time is close to 50 seconds, and with periodic conditions goes up to 3 minutes and 20 seconds. This difference is relevant only on implicit nonlinear simulations, as the building and inversion of the stiffness matrix happens at each step, whereas in explicit simulations and implicit linear ones, this happens only once, at the beginning. More on the difference between solvers will be explained in the next subchapter.

5.3 Solvers

The finite element method leads to a matrixial formulation of the elastic problem. These matrices can be quite large, with a number of degrees of freedom that can reach up to 10^5 or 10^6. For this reason, the computational process needs to be quick and not too expensive in terms of RAM and CPU usage.

In general, all the solvers calculate the solutions in a discrete number of steps, and at the end of each one the solution is outputted. A step can be subdivided in three phases:

- **Matrix building:** the first phase consists in the construction of the general stiffness and mass matrices (the mass matrix is not always required). These are built starting from the initial material data inputted, for the first step, or from the solution of the previous one. These information are then combined with the nodal connectivity of the elements, the boundary conditions, and the forces.
- **Calculation of the nodal displacements:** Depending on the type of solver, starting from the matrices, the nodal displacements are calculated. The method of calculation is what characterizes the type of solver. If the simulation involves accelerations and velocities, they are also calculated in this phase.
- **Material subroutines:** Once the nodal displacements are known, for each element, strains and stresses are calculated. This is done on the basis of the material law that has been specified for the element. In this phase, other data such as failure or softening are calculated, and then written on the output file and ready to be used as a starting point of the next step.

In the years, mainly two types of solvers have been developed in most commercial softwares: the explicit solver and the implicit one.

5.3.1 Implicit solver

The implicit solver is used for static or quasi static problems. It is based on the solution of the stiffness equation of the finite element method:

$$[K][u] = [F] \tag{42}$$

by inverting the stiffness matrix, and multiplying it by the force vector:

$$[u] = [K]^{-1}[F] \tag{43}$$

Once the displacements have been found, the material subroutines are initialized. This means that for each element, depending on the material properties, the nodal displacements are used to find strains, stresses, and all the requested information. This method can be used to solve linear and nonlinear problems, but with due differences.

The linear solver is characterized from the assumption of linear elastic material properties, so that the stiffness matrix is constant for the whole duration of the simulation. The stiffness matrix is built and inverted once, at the beginning, and displacements are found for each step by increasing the force vector. This means that material nonlinearities can not be accounted for, because it would be necessary to re-build the stiffness matrix to account for the change in stiffness. So, its use must be limited to the study of the elastic part of the response, as displacements can not be considered realistic after the nonlinearities sets in. However, if the simulation is brought after this point, it can display softening of the stress strain response, which is not realistic, but only the product of the non-linearities of the material cards. However, its quickness is useful in the first phases of the set up of the simulation, to debug the input file in the presence of problems and check the linear elastic modulus.

The nonlinear solver acts in a similar way, but, to account for nonlinearities, the stiffness matrix has to change depending on the material behaviour. Ideally, the stiffness changes continuously in time, but this can not be reproduced. The time is instead discretized in steps, at the beginning of which the matrix is reformed. This means that the real behaviour is approximated by a sum of linear steps. To ensure that each step is small enough and gives accurate results, convergence checks are made. These are conditions on the displacement, energy, and residual forces, which guarantee the correctness of the results with an acceptable margin of error. If these conditions are not met, the stiffness matrix is reformed or the time step is reduced. The reformation of the stiffness matrix is based on the previous step results.

In this case, the convergence was driven by two conditions. The first one is on the norm of the incremental displacement vector of the current step over the norm of the displacement:

$$\frac{|u_i|}{|u_{tot}|} < t_v \tag{44}$$

where t_v is a threshold value that has to be defined. The maximum norm is used, which is stricter than the Euclidian norm. The total displacement can be the imposed displacement on the single previous step, or the imposed displacement from the starting point. The first choice leads to a tolerance which is more stable at large deformations, because, as the simulation progresses, the total displacement norm denominator increases, and allows for greater residuals. On the other hand, some convergence problems were found with the norm based on the single previous step. It can happen that, with a strong softening behaviour of the material, or failure, the following step is greater in absolute value than the previous one. A greater displacement leads to greater residuals, and, if the difference between subsequent steps is large enough, the simulation fails to converge. As the norm is the maximum between all the nodes, a single element which undergoes failure or softening can give problems. This does not happen if the total displacement is considered, as the denominator is less sensitive to such changes. For these reasons, the choice in norm type depends on a case-to-case basis.

The default value for the tolerance is equal to 0.001, but it can be changed depending on the simulation. A stricter value ensures more accurate results, but also leads to a higher solution time, and such precision could not be needed. In this case, the tolerance was increased to 0.01. During simulation, this criterion has been proven the most critical one to satisfy between steps.

The other condition is the ratio of the incremental energy of the current step over the energy of the previous state:

$$\frac{E_i}{E_0} < p_{threshold} \tag{45}$$

the default value for the threshold is in this case 0.01, and has not been changed, as it has proven not to be problematic.

The main drawback of the implicit nonlinear solver is that the inversion and reformation of the stiffness matrix is a time expensive process. The time step is in this case important, as it affects convergence. Nonlinear solvers are useful for quasi-static problems, when the kinetic energy is low compared to the internal one, and for materials where nonlinearities are small.

From a computational point of view, the implicit solver uses a large amount of RAM memory, because of the inversion and reformation process, but a smaller amount of CPU time than the explicit.

The implicit solver can also account for the mass, by including the mass matrix in the computation, but this is not necessary for tensile tests and the study of the mechanical properties of materials.

5.3.2 Explicit solver

To solve problems in cases where the kinetic energy is predominant over the internal one, and nonlinearities are high, the use of explicit solvers is more adequate.

In these, the solution is not achieved by inverting the stiffness matrix but the mass one. The fundamental equation solved in this case is:

$$[M][\ddot{u}] = [F] \tag{46}$$

Once the mass matrix has been calculated, the parameters are lumped in the diagonal, so that the inversion of [M] is very quick.

$$[\ddot{u}] = [M]^{-1}[F] \tag{47}$$

Then, the accelerations are calculated depending on the force of the step, and the displacements are found integrating the acceleration and velocities. In this case, the single step has very small calculation times, as the stiffness matrix inversion is no more required, but the inertial components have to be taken into consideration. The main drawback of this method is that convergence is guaranteed by the time step itself, as it has to be smaller than the time at which information travels inside elements (speed of sound). This implies the simulation time dependence on the size of the mesh, densities and Young's moduli of the materials. The time step can be calculated approximatively as:

$$\delta t \approx \frac{l_{element}}{c} \approx \frac{l_{element}}{\sqrt{E/\rho}} \tag{48}$$

where:

- $L_{element}$ is the characteristic length of the element. This is represented by the ratio between the volume and the smallest surface area of the element. The bigger the element, the longer time the sound takes to cross it. It is directly proportional to the time step, so a finer mesh slows down the simulation compared to a coarser one.

- c is the speed of sound in the material, which is proportional to the ratio between Young's modulus and the density. The higher the stiffness, the smaller the timestep, and the higher the mass of the element, the faster the simulation goes.

The time step is calculated for each element, and the smaller one from all is taken as the maximum limit.

From a computational point of view, the explicit solver is the opposite of the implicit one. The time steps are much smaller, but quicker. The allocated amount of RAM is lower than the implicit analysis, but the CPU usage is far greater.

The fact that the number of time steps is high, and can reach up to 10^4 or 10^5, justifies the choice of elements with a underintegrated formulation, as the importance of a fast material subroutine increases whit such number of steps.

This dependence of the simulation time from the materials and the mesh can be problematic, especially if a fine mesh is needed or the material has a high stiffness-to-density ratio. For these cases, a technique called mass-scaling has been developed. This technique artificially increases the overall mass matrix of the system by placing fictitious masses in places of the matrix that do not affect the solution.

As the simulation now involves the inertia factor, but the tests are static or quasi-static, it is important that the dynamic forces are negligeable. A good norm is to check that the kinetic energy of the system is much lower than the internal one, at maximum 5%. To reduce the kinetic energy, it is necessary to have a global simulation time long enough, so that the velocities of the nodes are small enough.

5.3.3 Comparison between solvers

As said before, the implicit linear solver has proven to be helpful in the first phases of the set up of the simulation. As the stiffness matrix is inverted only once, the solution time is the smallest of all three solvers, with a run time of about 7 minutes. This solution was helpful in the debugging phase, to correct mistakes, check the correct application of the boundary conditions, and the linear elastic behaviour of the model.

The explicit solver was the first choice for obtaining the definitive solutions. But, as already said, the implementation of periodic boundary conditions was unsuccessful.

Another problem with the explicit consisted in the deletion of elements that failed for negative volume. This happened because of the change in equilibrium forces at the nodes of a delete deleted element. At the step before deletion, the node is subjected mainly to elastic forces, of roughly the same intensity, but opposite in direction. Once the element is deleted, the equilibrium is no more present, and the node starts accelerating towards the element next to the deleted one. This inertial effect is so large that the element is compressed and fails. This starts a chain reaction that erodes elements in an unrealistic way. This behaviour can be mitigated by including damping and controlling the post failure stress-strain curve of the material, to smoothen out the sudden stress jump. In this case, the effect was still present and could be seen near the constrained faces of the RVE. Even

if these faces were modelled with an elastic material to remove the boundary effect, the problem was still present.

At last, by doing a simulation with the implicit nonlinear solver, linear kinematic boundary conditions did not assure the right behaviour, as the results were different than the model with periodic boundary conditions. The RVE size was too small to converge with these constraints.

For these reasons, the explicit solver was discarded. It has to be said that, with proper mass scaling, element formulation "1", and hourglass method number four or five, the simulation time was close to 40 minutes, which is good for such big simulations.

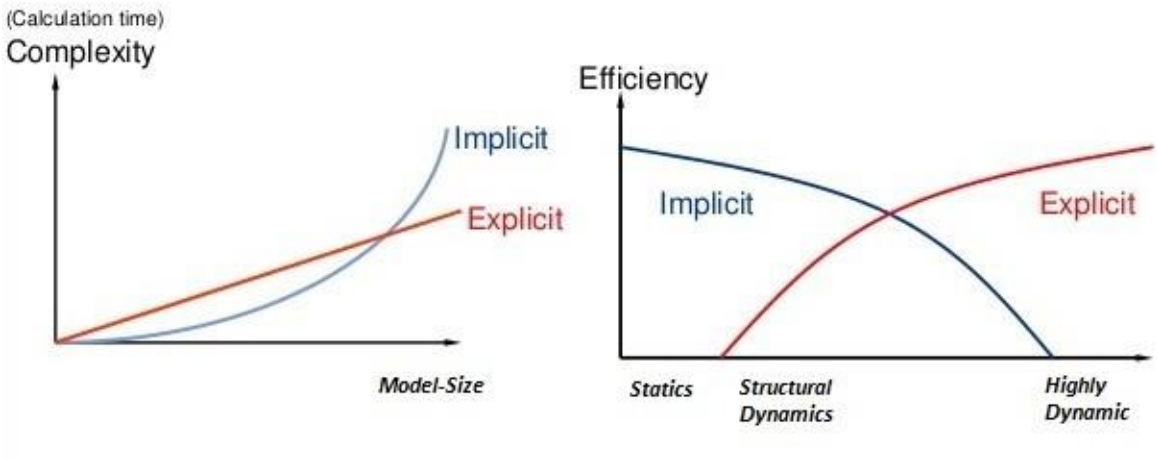

Figure 14 – General remarks on the difference between explicit and implicit simulations

The implicit nonlinear solver was the final choice, due to the problems with explicit. The main challenges of this are the long simulation times, and the convergence checks. To speed up the simulation, it would be necessary to increase the time step, reducing iterations. But, at the same time, a too large step can prevent the solution from converging; a trade off must be found.

A smart strategy is to impose an initial large step, to cover the majority of the linear elastic part, as it does not create difficulties on the convergence. Then, a constant step can be imposed, but still allowing the software to automatically adjust the step.

As regards the convergence thresholds, a trade off has to be found between accuracy and time. In this case, it is recommended to look at the iterations, the norms of each one, and the solution. For example, if a lot of iterations have a norm ratio close to the threshold, and this leads to a reformation of the matrix, it is possible to slightly increase the limit. A similar effect is achieved by changing the calculation of the norm ratio, from current step displacement to total displacement. A critical look at the solution can also help identify the opposite case, when the threshold is too large that non correct solutions have converged. This is observed as overshoots in the material stress strain curves, where the stress is much higher or lower than expected, or non-physical behaviours.

5.3.4 Post-processing techniques

The post-processing phase consists of extracting the results of interest and check the quality of the solution. In this case, some technique and practices were implemented.

To create the stress-strain curves, the correct procedure consists in calculating the weighted sum on the volume for each element. For each frame:

$$\sigma_{frame} = \frac{1}{V_{tot}} \sum_{i=1}^{n} \sigma_i V_i \tag{49}$$

And the same goes for the strains. This has been done with a MATLAB™ script, which takes in input a text file exported from LS-Dyna™ and performs this transformation for each frame. As cubic elements of the same size have been used, the volume weight is the same for all, so the global stress value reduces to the mean value of all elements. If the element formulation is '1', with a single integration point, Ls-PrePost™ outputs the value of that same point. If more than one integration point is present, an average value between them is outputted. The total volume is defined as the totality of the material subjected to the study, so, in case of RVE with voids, they also have to be accounted for the calculations. This calculation technique is called homogenization.

Another technique that has not been used in this case is to evaluate the displacement of the dummy node, divide it by the total length of the specimen, and calculate the true strain with the logarithm.

As said before, voids were modelled as elastic elements with a low young's modulus. To ensure that these elements did not influence the results, the stress values should be at least two orders of magnitude lower than the average stress. In this case, maximum stress values did not overcome 10^{-1} MPa, which is acceptable, with global stresses averages as high as 60-70 MPa.

The evaluation of the failure mechanisms has ben done with the help of the additional integration point storage. With the keyword *DATABASE_EXTENT_BINARY, additional integration points can be requested. These have not a role in the calculations, but store helpful values, depending on the material card used. For example, in composites models, these points store the failure index of a certain criterion. This helps to understand which criteria in which part of the RVE has failed earlier or later, and understand the global behaviour of the model. Usually, these failure indexes are equal to one if the criterion has not been reached and drop to zero when failure happens in that mode.

5.4 Digital image correlation

Digital image correlation (DIC) is a technique used to map the strains of the material in load tests. It is based on the assumption that the surface displacements are equal to the internal ones, and so the mapped strain field from images is comprehensive of the whole material under load.

It works by using a high-resolution camera pointed at the specimen. Then, points are assigned to the surface, elements are defined between them, and their movement is tracked along the test. The result is a visual mesh of elements and nodes that moves in time. Then, based on the displacement of such nodes, the deformations are calculated.

The main advantage of this procedure is that allows to get a field of displacement along all the specimen, and better evaluate difference in strains that can appear inside the specimen in some cases, like necking. This is not always possible with other, more traditional methods. For example, calculation by means of the crossbar movement can only evaluate a global deformation, and is subjected to the error of including the deformation of the clamping mechanisms. Using a strain gauge also measures deformation in only one point, which must be chosen before the test, and not always coincides with the necking point. Strain gauges are also affected by temperature effects.

The main drawback of the DIC method is its cost, as high-resolution camera is needed and the software can be expensive. A schematic representation of the hardware needed in DIC techniques can be seen in Figure 15.

This is the method used for obtaining the stress strain curves of the matrix and the specimen.

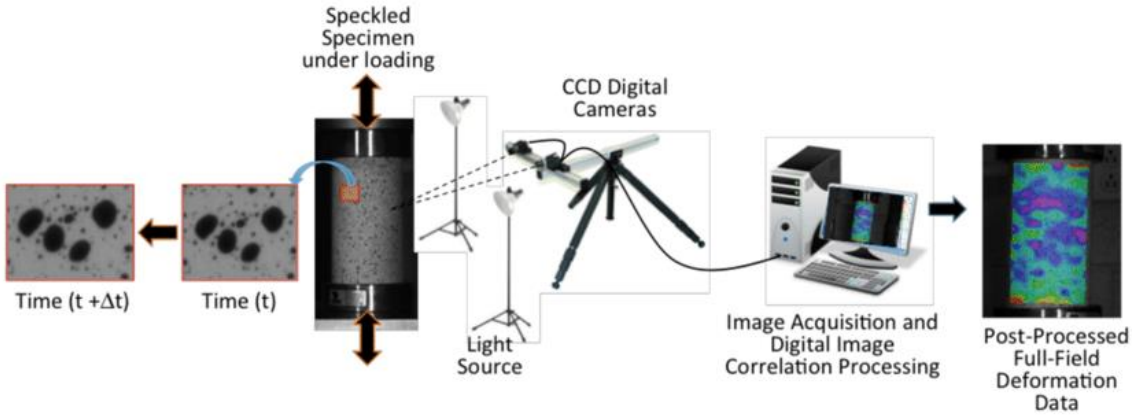

Figure 15 – Schematic representation of the DIC technique

5.5 Server data

As the computational speed is not only dependent on the optimization made by the user and the software, here there is general data about the server used for these simulations. This is useful to fully evaluate how much of the simulation speed is due to optimization, and how much to the computational power.

- **CPU:** 40 cores, speed of 2.59 GHz. For the simulations, only 24 were used.
- **RAM:** 63.4 GB, each core uses at maximum 1.71 GB. Peaks of 30 MB were used in the implicit simulations.

6 Failure

While elastic properties are easier to investigate, the main challenge lays in the simulation and numerical prediction of the failure mechanisms. This is especially true for composite materials, as the failure behaviour is governed by different modes, and correctly identifying and simulating all of them is a very difficult challenge.

The failure in ±45° angle ply composites is driven by various factors. The stress-strain response of tensile tests shows a pseudo-elasticity, which is very different from the usual brittle failure of composites. This is due to the microstructural changes and failure mechanisms that are present inside the constituents. The stress-strain response can be generally subdivided in three phases:

I. **Linear elastic response**: in the first part of the curve, the tensile response is given by the linear elasticity of the constituents. The overall stiffness is a sum of the contributions of the elasticity of the matrix, the lateral elasticity of the tows, and the longitudinal elasticity of the fibres. As the pure matrix has the lowest Young's modulus of all these three contributions, this constituent holds a higher deformation than the other two. For the same reason, the deformation in the lateral direction of the tow is higher than the longitudinal one.
II. **Plateau**: As stresses increase, the yielding limit of the matrix is reached. This yielding usually appears first inside tows, as fibres act similarly to a notch, and a stress intensification phenomenon appears. This causes cracks formation and the onset of the matrix inelasticity.

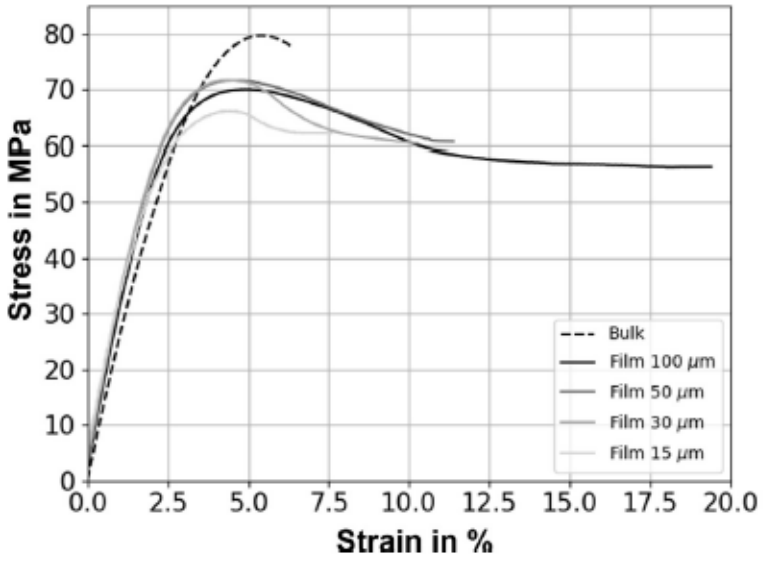

Figure 16 - Summary of the experimental results of tensile tests of epoxy resins, with thicknesses of 15, 30,50,100 µm.

This phenomenon is a result of the scale sensitivity of epoxy resins. It has been shown in [15] that resin specimens with a small thickness have a much higher ultimate strain than the bulk ones. This could be explained by a reduced number of defects inside the microstructure, which allows sliding between polymeric

chains. This justifies the choice of a material card with a failure strain of 20%, which is close to the results given in the aforementioned study.
Experimental results of the study [15] can be seen in Figure 16.
Inelasticity of the matrix inside tows leads also to another phenomenon, which is the fibre re-orientation. Similarly to what happens in the microstructure of the epoxy resin, the inelastic phase allows for the fibres to rotate towards the load direction.
As these changes in the microstructure happen, new cracks are formed and propagate. Cracks usually starts from the intra-tow matrix, for the same notch effect of the fibres; then, they propagate in rich resin zones.

III. **Potential stiffening of the response and failure**. With certain types of matrices, a microstructural rearrangement of the polymeric chains leads to a re-stiffening of the matrix; this phenomenon strongly depends on the nature of the polymer. Considering also the re-orientation of the fibres, the new microstructure is stiffer than the previous one, and this leads to an increase in the slope of the stress-strain curve.
However, the crack propagation phenomenon is still in place, and damages the matrix. These two opposing events compete with each other, and depending on the material, one of them is prevalent on the other.
The final failure of the whole composite can be led by longitudinal fibre breakage or matrix damage due to cracks, depending on a case-to-case basis.

As it can be seen in this example from Figure 17, the first phase ends at the point N, the second one starts from N until point P, and the third phase ends at failure. Even if the

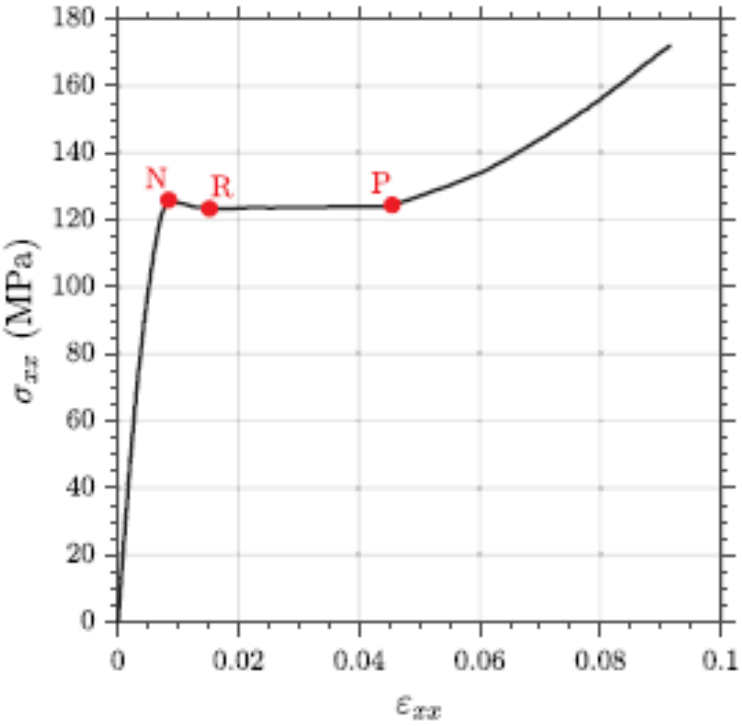

Figure 17 - Example of the three phases response of a CFRP composite.

example regards a carbon fibre reinforced composite, the failure mechanisms are the same. The difference lays in which behaviour is prevalent on the others.

To investigate which mechanisms are prevalent in the tested material, an analysis of the tensile tests results in Figure 18 is needed:

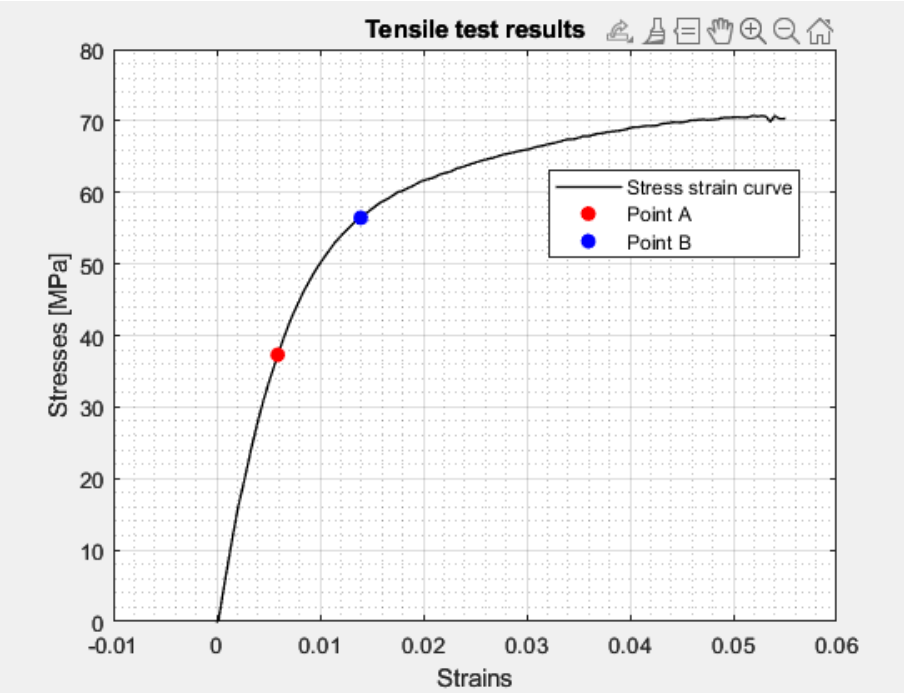

Figure 18 - Empirical results of the tensile test

Up until point A the response is mainly linear, which leads to conclude that we are in the first phase, on the basis of the considerations made in [15]. After that point, the nonlinearity becomes evident. This can be due to failure of the matrix inside tows, and propagation of intra laminar cracks. Then, after point B, the damage is expected to propagate in rich resin areas, as the matrix enters his plasticity phase and cracks propagates. This damage is expected to be counteracted by the fibre re-orientation, but it could be a small contribution that leads to the slight increase in stress in the final phase.

To identify these failure mechanisms, the following indices have been defined:

- **Tow failure index**: the material card 054 allows to store failure information for each integration point of the elements. The failure flag is either zero, i.e., failure occurred, or one, i.e., no failure.
  By using this information, a global damage variable can be calculated, as a mean value of all the failure flags in the tows. This procedure has been applied to the matrix failure flag, to track the intra tow cracking formation.
  In this case, a global damage variable equal to zero means that all the elements are still active in the lateral direction, while a variable equal to one means that the matrix has fractured in all elements.
- **Fibre failure index:** the same procedure applied to the matrix failure inside tows has been adopted to the fibre failure. The damage variable is calculated in the same way and has a similar meaning.

- **Matrix failure volume fraction:** to track crack propagation in the pure matrix zones, a different approach has been used. In this case, the plastic strain has been chosen as the variable of interest. An element of pure matrix is being deemed as damaged if the plastic strain exceeds the value at the peak of the material curve, where necking starts (see Fig. 5). By counting elements whose plastic strain is higher than the chosen threshold a volume fraction of damaged matrix can be calculated.

Other important information that can be visually retrieved by the simulation results are the location of the elements with the highest plastic strain. These are located near voids, especially at the boundaries between voids, matrix and tows. This is coherent with the literature, as voids are expected to facilitate crack propagation and damage.

7 Simulation parameters tuning

Once the initial simulation set up has been realized from previously made assumptions and considerations, the work shifted onto the optimization of the procedure and correction of the parameters. As a lot of the choices that have been made are a result of a trial and error procedure, and depend on the correlation between parameters, they will be explained in this chapter.

7.1 Tow parameters

As seen in the material section, some of the parameters of the card do not have an experimental procedure which allows their predictions. One of these parameters is the shear factor beta, which influences tensile driven failure.

$$\left(\frac{\sigma_{11}}{X_t}\right)^2 + \beta\left(\frac{\sigma_{12}}{S_c}\right)^2 = f_1 \tag{50}$$

The influence of the shear stress in fibre driven failure is still a debated topic, so there are not recommended values for β. If β is equal to zero, the failure criterion is that usually referred to as the maximum stress theory. Else, if β=1, the criterion coincides with Tsai-Wu. As seen in [17], the choice is case dependent and can be addressed through a trial-and-error process. In our case, a good agreement was found for β=0.65. This influence of shear could be explained by the fact that the stress field is made up of different components, such as shear deformation, tension on the fibre, and on the matrix. This can unleash different failure mechanisms such as debonding and decohesion, whose effects are underestimated by the maximum stress theory, and overestimated by Tsai-Wu Criteria. To have a better estimation of β in different load conditions, a micromechanical investigation would be necessary, similarly to what has been done in [8]. Even if the load conditions considered in the research were very different from the one present in this case, it can be observed that several failure criteria can give large differences between actual and predicted results, which justifies an empirical estimation of β.

A similar parameter to β is α, the nonlinear shear term. It introduces a factor k equal to:

$$k = \frac{1 + \frac{3}{2}\alpha G_{12}\sigma_{12}^2}{1 + \frac{3}{2}\alpha G_{12}S_c^2} \tag{51}$$

Which multiplies the shear component in the fibre failure criteria.

$$\left(\frac{\sigma_{11}}{X_t}\right)^2 + \beta\left(\frac{\sigma_{12}}{S_c}\right)k^2 = f_1 \tag{52}$$

It has been decided to neglect this value and put it equal to zero. The shear influence would be driven only by β, as it is simpler to tune, and the higher precision of α did not bring considerable advantages.

Another parameter that had to be chosen was the post failure stress of the matrix. With the option SLIM, a reduction factor for the limiting stress can be specified. A value of 1

leads to a perfect elastic-plastic behaviour, and a value of 0 to a fragile fracture. If the fragile behaviour in the longitudinal direction has been undisputed, the behaviour of the matrix, which means the limiting factors in shear and lateral tension, is not so trivial. As said before, the ductile behaviour of epoxy resin at the microscale could justify perfect plasticity after failure. At the same time, due to the significantly different stiffness of the constituents, fibres determine stress intensification and to a triaxial stress state in the surrounding matrix, which trigger a fragile behaviour.

In this case, the second effect, i.e., the stress intensification and the resulting fragile failure, was deemed prevalent on the first one, i.e., the intrinsic plastic behaviour of the matrix, and a good agreement with empirical data was found.

As regards fibre rotation, Ls-Dyna™ tracks the change in material direction only considering rotation of the element, by default. In the card 022 the option "ATRACK" allows to consider the deformation of the element into the calculation of the orthotropic properties. This is done by taking two points on the element at the beginning of the simulation, so that the material axis goes through them. Then, as deformation are imposed, the points are tracked and the material axis orientation is updated. This option slows down the simulation, as the process is computationally expensive.

As the fibre rotation is a phenomenon present in 45° laminate composites, this option would help achieve an accurate result. However, the option is available only for shell elements.

Other material parameters of the card 054 are the DFAIL for tensile, shear, and lateral deformations. These allow to specify a certain amount of strain after which the element is deleted. These resemble the maximum strain criteria. In this case, they were not taken in consideration, to simplify the optimization process. A similar parameter, which has also been ignored, is the EFS. It imposes a maximum effective strain, calculated as a Euclidean norm between the tensile strains in the longitudinal and lateral dimensions, and shear.

*MAT_ENHANCED_COMPOSITE_DAMAGE_(TITLE) (054/055) (1)

	TITLE							
	Fibre 054							
1	MID	RO	EA	EB	(EC)	PRBA	(PRCA)	(PRCB)
	54	2.210e-06	5.200e+04	4145.0000	4145.0000	0.0195000	0.0195000	0.3500000
2	GAB	GBC	GCA	(KF)	AOPT	2WAY	TI	
	1540.0000	1537.0000	1537.0000	0.5700000	0.0	0.0	1.0000000	
3	XP	YP	ZP	A1	A2	A3	MANGLE	
	0.0	0.0	0.0	0.0	0.0	0.0	0.0	
4	V1	V2	V3	D1	D2	D3	DFAILM	DFAILS
	0.0	0.0	0.0	0.0	0.0	0.0	1.0000000	1.0000000
5	TFAIL	ALPH	SOFT	FBRT	YCFAC	DFAILT	DFAILC	EFS
	-0.1000000	0.0	-0.1000000	0.4000000	2.0000000	1.0000000	-1.0000000	1.0000000
6	XC	XT	YC	YT	SC	CRIT	BETA	
	1051.0000	1529.0000	22.200001	22.200001	14.940000	54.0	0.6500000	
7	PEL	EPSF	EPSR	TSMD	SOFT2			
	100.000000	0.0087000	0.0090000	0.9000000	1.0000000			
8	SLIMT1	SLIMC1	SLIMT2	SLIMC2	SLIMS	NCYRED	SOFTG	
	0.0200000	1.0000000	0.0500000	1.0000000	0.0500000	1.0000000	1.0000000	
9	LCXC	LCXT	LCYC	LCYT	LCSC	DT		
	0	0	0	0	0	0.0		

Figure 19 – Example of material card data for MAT_054

Crashfront softening parameters were also ignored, as they are useful in dynamic simulations of crashes, to stabilize the solution. Other remaining variables were set to the default values, where possible, or ignored. Figure 19 shows all the parameters present in the material card 054.

7.2 Displacements

The correct definition of the displacements in an RVE simulation is not as trivial as it seems. In this case, a load curve has been defined, which represents the global deformation of the material. Then, the curve has been referenced in the prescribed motion, and its values were multiplied by the length of the RVE.

In the case of the tensile test, the sole definition of the longitudinal displacement led to unrealistic solutions. Results gave a value of the Young's modulus of half the real one, and a Poisson's ratio of around 0.72. The problem was solved by imposing a lateral compressive motion, which resembles a global Poisson modulus, with a value of 0.378. This number has been found iteratively, by looking for convergence between the simulated and real Young's moduli. For the out of plane direction, the RVE has been left free to move. This is because the dimensions of the RVE account for 10 out of 12 layers, and neglect only one lamina at each side. For this reason, that the assumption that out of plane surfaces of the RVE behave like the free surfaces of the laminate is acceptable.

7.3 RVE shape

The RVE initially chosen has a pseudo-cubic shape, with the two in-plane dimensions equal to 6.1 mm, and the out of plane one limited by the number of layers to 5.5 mm. After some attempts, it was noted that the behaviour of the cubic RVE showed a more brittle behaviour than the specimen (Figure 20). The simulation ended with errors and stopped

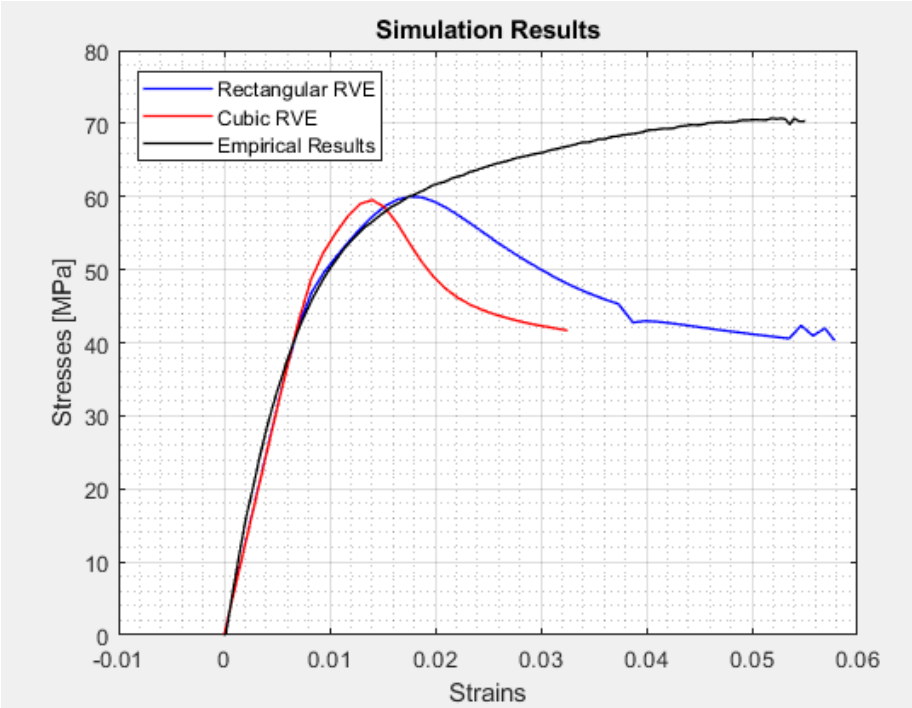

Figure 20 - Comparison between the cubic RVE and rectangular RVE, with identical parameters.

before reaching the imposed deformation. This behaviour was attributed to the main tow on the diagonal, which has elements in connection with x and z direction faces. A hypothesis has been made, and stated that, because the main tow is connected to both faces where the displacement has been imposed, the longitudinal stiffness of such tow played a greater role than it should have. In fact, in the real specimen there are not tows that cross the entirety of the length. This hypothesis has been confirmed when an attempt with a rectangular RVE was made. The difference can not be attributed to the porosity, as the void volume fraction of the cubic RVE is greater than the rectangular one (1% against 4.16%, respectively). The rectangular RVE has been chosen with a length of 9.1 mm, and a width of 4.1 mm. These numbers were chosen to ensure the absence of the cross-sectional tow, and to have a similar number of elements (205205 against 204655).

This new rectangular RVE (Figure 21a) will be used in the simulations.

This difference suggest that the RVE which is capable to describe the elastic behaviour of the material not necessarily coincides with the one capable of describing failure. Therefore, this aspect should be furtherly investigated in the future, to asses the dimension and shape of the RVE necessary to characterize material failure.

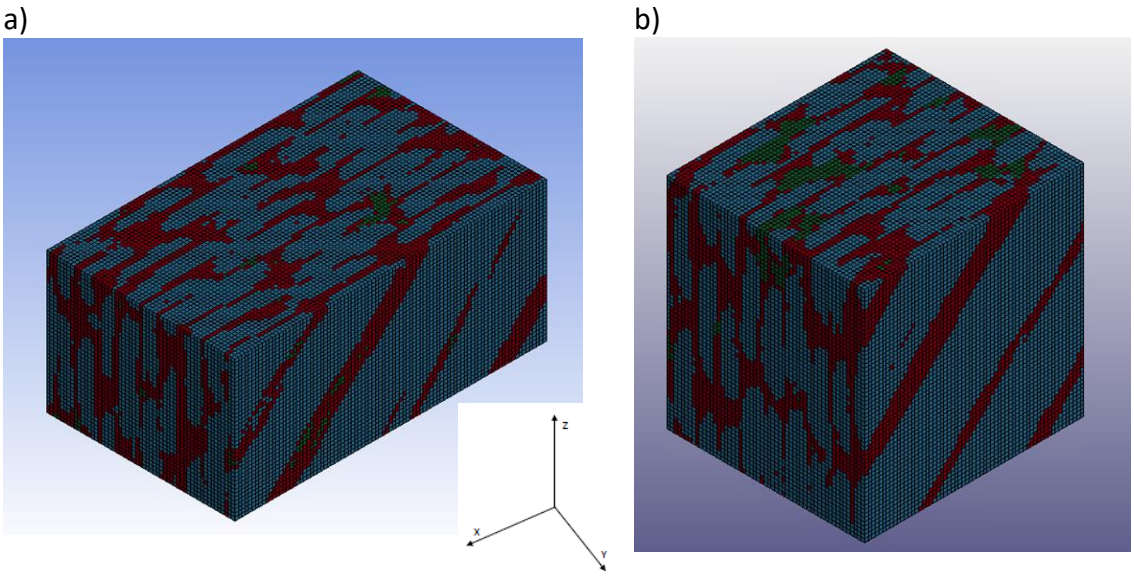

Figure 21 - Image of the new rectangular RVE against the cubic RVE

7.4 RVE extraction and preparation

The extraction of a statistically significant number of RVE's is a process that can be time consuming and must ensure a full coverage of the defects inside the material. For this reason, a Matlab™ script was developed to automatically extract a random RVE, mesh it, and write a boundary conditions file. This puts together smaller functions, which have different origins. The random extraction function was already developed in the DIMEAS database, as well as the boundary condition writer, which needed only an adaptation in syntax from Abaqus™ to Ls-Dyna™. The mesher was found online, in the Matlab™ file exchanger [13].

Then, after the final parameters of the simulation have been established, a general RVE file has been produced, which contains all the necessary keywords. The only things that were not automated were the assignment of material orientation to the elements, and some small correction. As for the first one, it would be technically possible to assign orientation automatically, similarly to what has been done with the boundary conditions. The other small corrections were due to some standard keywords that Ls-Dyna™ automatically includes in the file, which needed to be eliminated, and renaming of other files. This procedure did not take more than 15 minutes for each RVE.

Another key point was the number of RVE that should be simulated. The goal is to account for most of the defects inside the material, but also to have a short total simulation time. An estimate was done by dividing the total number of voxels available from the CT scan to the RVE size. As there are 1 396 010 voxels in the original file, and the RVE size is equal to 205205, the ratio between these numbers is about 6.8; so, seven RVEs were simulated. As the extraction is random, it is not possible to account for all the defects in the material without accounting more than once for some other voids. A better option would be to manually choose the RVEs in such a way that all the defects are considered.

As regards the perfect RVE, a quick correction has been made on the mesh. Despite the fact that TexGen™ could output an STL or IGES file, which could be re-meshed externally with another software, an Abaqus™ voxel file has been exported. This has been done because it is simpler, and to use a similar mesh to the real RVE's, to eliminate variabilities in the results which could be attributed to the difference in elements. The final mesh is identical to the one used for the real RVEs, and the shape has been changed into the rectangular one, while still retaining the original assumptions on tow sections and volume fractions.

A problem arose during the simulations, as it was noted that the tows inside the pristine model were all connected together and not separated by the matrix. This led to a brittle behaviour in the results. The problem can be attributed to the interpolation procedure of TexGen™ in the mesh building phase; the fibre bundles were modelled as an ellipse, and to transform the round edges into faceted surfaces, the elements at the boundary have to be assigned to either tows or matrix. Probably, all boundary elements were automatically assigned to the bundles. The problem was solved by correcting the mesh by hand, reassigning the elements to the correct part.

7.5 Fibre orientations

The fibre orientation has to be assigned to the tow elements, as they have orthotropic properties. In Ls Dyna™ there are two ways to assign element orientation:

- Direct assignment with the AOPT options in the material card. There are up to four options, which allow the assignment to be made via vectors, points, or angles. In this case, if the same material has two different orientations, different cards and parts have to be defined.
- Assign the orientation to the elements and leave the AOPT blank. This was the chosen procedure, simply because it required less steps.

The problem with the real RVEs was that the hand lay-up process led to adjacent tows of different orientations, and not well-defined layers. For this reason, an accurate assignment of around 120 000 element orientations has been deemed impossible, and the layer division is made by only evaluating the tows at the surfaces. It is assumed that errors in the procedure are present, but as the ±45° orientation are perfectly opposite to each other, these errors counter-balance and lead to a final accurate estimation. Considering that this imprecision is present, the automatization of orientation assignment has not been done, as it probably introduced further errors. Also, the assignment procedure is not so time consuming.

7.6 Solver parameters

To get a simulation which runs smoothly and comes to a correct solution in an acceptable amount of time, parameters have to be chosen in a case-to-case basis, depending on element behaviour, geometries, and so on.

For the matrix, the final card chosen was the 081, as the post failure damage needed to be specified. As said before, this card could lead to some numerical instabilities for high damage levels. To avoid these, the failure has been modelled as follows.

- The empirical curve has been followed up until failure.
- Then, a sudden jump of damage value from 0.33 to 0.9, to reduce the residual stresses.
- Then, a constant damage evolution has been imposed. This leads to a residual stress of around 8 MPa, which can be neglected. The damage never falls below this threshold, to prevent numerical instabilities.

This choice of post failure evolution has been made together with the choice of the norm “2”, the one calculated over the total displacement. The difficulties in convergence remained when some elements close together reached a damage value around 0.9, with the use of the current step displacement norm. As explained before, the sudden change in elasticity is problematic for the norm “1”, but not for the “2”. The only drawback is that, at the end of the simulation, stress oscillations could be seen (Figure 22), as a result of premature convergence already explained. These oscillations are acceptable, and do not change the general behaviour of the response.

Another important choice is the norm tolerance, especially the displacement one, which has been proven the most difficult to satisfy. To tune in this parameter, some tries have been made by increasing and reducing the threshold and seeing the effects on the quality and speed of the simulation. It has to be large enough to get to a solution in a reasonable amount of time but also give accurate results. In this case, a threshold value of 0.01 has been chosen.

Another important parameter is the maximum stiffness reformation limit. After the solver fails to reach equilibrium, it rebuilds the matrix, on the basis of the previous attempts. After a certain number of stiffness reformation, the solver decreases the step time. In this case, a peculiar behaviour was noted: if the first attempt did not achieve equilibrium,

other reformations were always unsuccessful, until step time reduction. For this reason, the reformation limit has ben set to one, the lowest available number, to spare the solver from all the unsuccessful reformations.

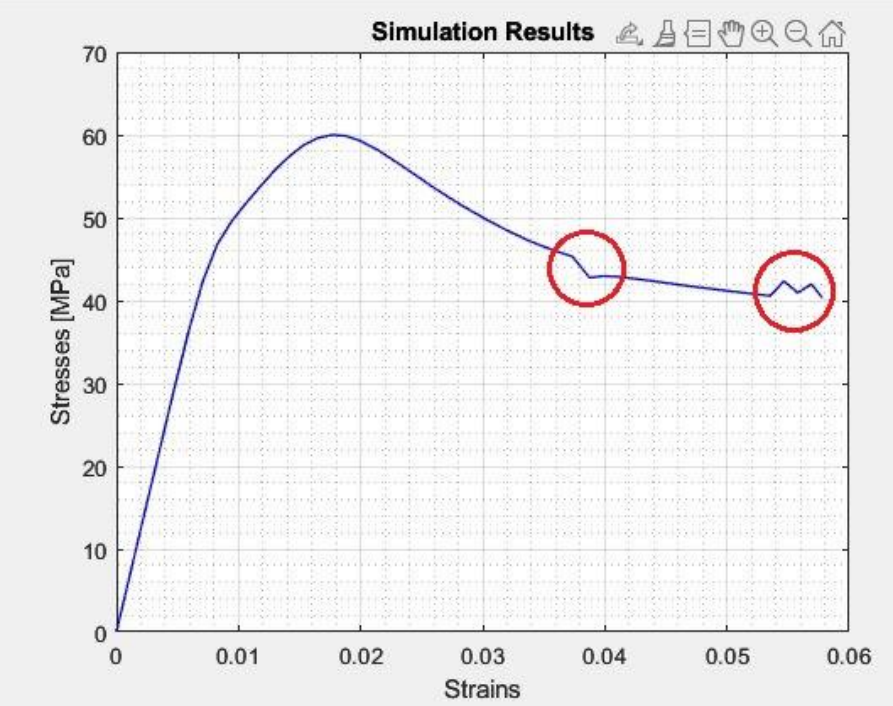

Figure 22 - Numerical oscillation in the results, circled in red

To analyse the results in a meaningful manner, it is necessary to get curves with an acceptable number of points. This influences the solution time, as a greater discretization needs more step calculation. In this case, an optimal equilibrium was found with 48 steps. The first two were bigger, double the amount of the others, as it was observed that they were in the elastic regime, and in that part high discretization is unnecessary. As mass is not involved, and accelerations are not computed, the total time had not physical meaning, so the choice is, in this case, arbitrary. It is convenient to choose a round number, like fifty or one hundred as the total time, and then discretize all the steps from there. For this simulation, the total time chosen was one hundred, with the first two time

RVE n°	*Simulation time*
1	1 hour 43 minutes
2	1 hour 15 minutes (failed to converge at 80%)
3	1 hour 38 minutes
4	2 hours 15 minutes (failed to converge at 92%)
5	2 hours 4 minutes
6	1 hour 46 minutes
7	2 hour 22 minutes

Table 5 – Resume of simulation times

steps equal to four, and all the others to two.

The choice of the elements has been made similarly to the choice of the threshold, by looking at the quality and time of the simulation. As said before, it is usual that implicit nonlinear simulation benefit from high accuracy elements, like “-1” and “-2”. The choice

fell on the simple one integration point element (element formulation #1), which is faster than the others, and gave acceptable results. Other elements created stability problems and prevented simulations to come to a correct termination. All but two simulations reached the normal termination, and those who did not fell short to accomplish it. The differences between simulation times and convergence issues can be due to instability in the matrix elements. A mean simulation time of 1 hour and 55 minutes has been measured from the five runs that reached correct termination.

8 Results

The extrapolation of the final results focused not only on the stress strain behaviour, but also on the analysis of all the failure modes of the model, and the comparison between the empirical observations and the simulated behaviours of the RVEs.

Starting from the results of the single simulations (Figure 23a), a median curve between all the RVEs has been computed (Figure 23b), which represents the average behaviour of the as-built material. The same thing has been done for the damage variables of the real RVEs (Figure 24).

a) b)

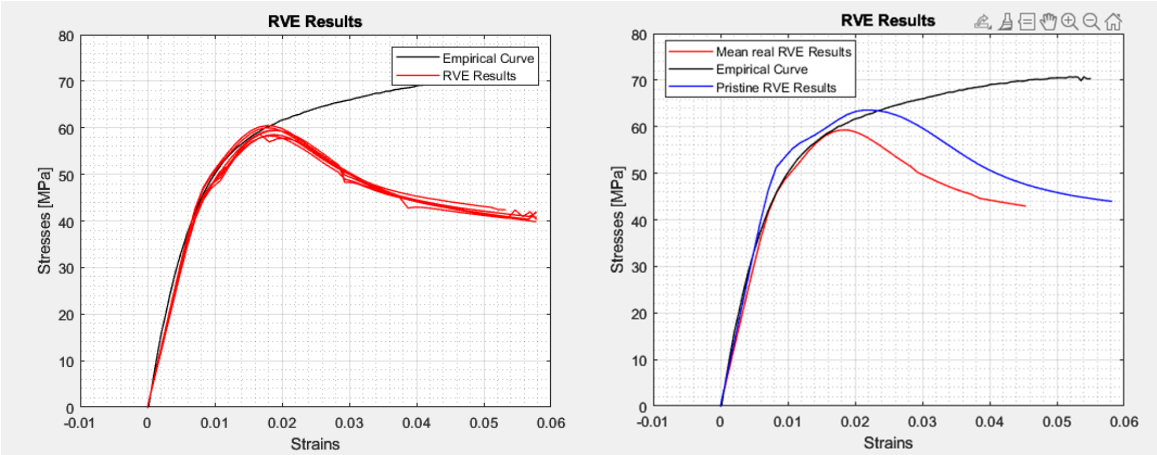

Figure 23 – Average curve of the RVE test extracted from multiple simulations (a) compared with the experimental results (b).

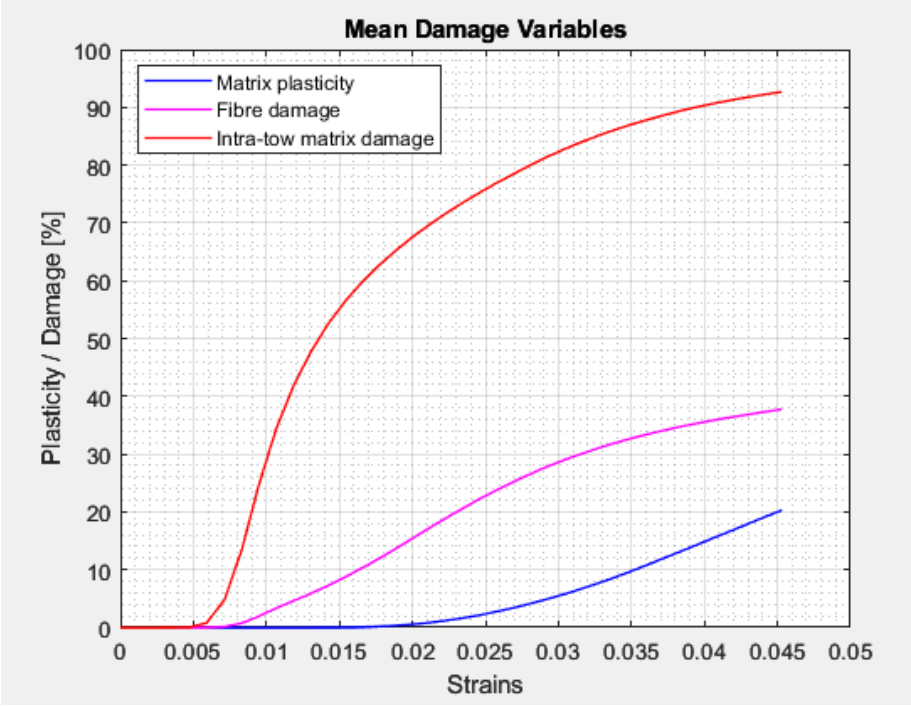

Figure 24 - Averaged damage variables between all the real RVEs simulated

All the simulations show a softening behaviour, which starts around 2% of the total deformation. To further investigate the causes of such behaviours, a critical analysis of the damage variables is necessary.

Figure 24 shows that:

- The first damage happens in the matrix inside the tows, due to the fact that the notch effect of the fibres lowers matrix ultimate strength. This is coherent with the experimental observations as it represents the first cracks that appear between fibres. This damage starts to affect the stress-strain behaviour around 1% of total deformation, where the first softening of the curve appears.
- The second damage that appears is the longitudinal tow variable. It is not as significant and sudden as the intra-tow matrix one, and seems to slightly affect the stress-strain curve just before the 2% deformation mark.
- The third and last damage is the plasticization of the matrix. It is the latest to start, but bears the most significant effect of all As soon as the first matrix elements start plasticizing, the stress-strain curve starts to soften, and deviates from the empirical behaviour.

This can be explained by looking at the locations where the matrix damages in Figure 25.

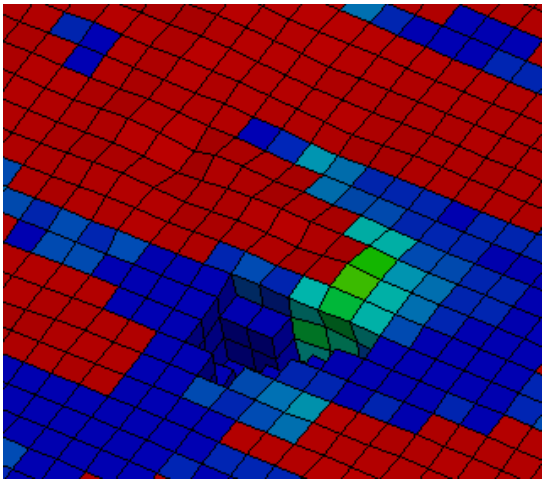

Figure 25 - Details of the plasticization of the matrix around the tows. The plasticized elements (in green and light blue) are concentrated near the tows (in red), while the rest of the matrix is undamaged (in blue).

It can be noticed from Figure 24 that the damage of the matrix starts just after fibre failure. This can be explained because the failure of the tow in both matrix and fibre leads to bundle zones with low residual stiffness. These zones act like notches, and a stress concentration phenomenon appears in the matrix around them. The resin starts then to enter its plasticity phase. This finally leads to large inelastic strains, which prevent the matrix from conveying the load to the tows that are still active in the fibre's direction. In the final phases, as the active tows stop to bear load, the curve tends towards the damage behaviour of the pure epoxy resin.

This can also be observed by looking at the slopes of the damage variables. The fibre failure precedes the matrix plasticization, and once this starts, the slope of the fibre failure index decreases. This can be due to the fact that the tows are not anymore under tension, because all the strain concentrates in the inelastic parts of the matrix.

At the end, the amount of fibre failed does not exceed 38%, which means that most of the fibres are still active, and did not break because of the relaxation of the matrix around the tows.

8.1 Notch effect around tows

As described earlier, the final part of the stress strain evolution is affected by a notch effect around tows, that generates large amount of matrix inelastic strains and overcomes the damage of the tows, leading to a macroscopic softening effect. This is not an empirical phenomenon, but, at the same time, is correct from a computational point of view. The problem lays in the discretization error of the model.

Near the boundary zone between matrix and tows, there is a very high difference between elements with different elastic properties and failure models. The epoxy resin has a Young's modulus of 3000 MPa, and its tangent modulus reduces to zero over a large amount of strain. On the other hand, tows are much stiffer and have a brittle failure, leading to a drastic change in elasticity. This can cause the notch effect, which in this case appears as the tows get damaged and lose all their capability in holding stress, acting like a void. In the real specimen, this transition is not so sudden, and a crack propagation phenomenon from intra tow zones to the matrix is observed. It can be concluded that this notch effect is the numerical approximation of the real crack propagation phenomenon from one zone to the other. As the discretization of the elements is too large, and the boundary between different zones is sharp, the real stress-strain behaviour can not be interpolated.

To get a smoother transition between tows and matrix, three actions could be taken:

- A more accurate CT scan of the specimen, which translates to a more expensive machine and procedure.
- A more accurate discretization of the intermediate zone, by means of more elements. This would affect simulation times and be more computationally expensive.
- A more accurate phenomenological description of the intermediate zone, with material properties that interpolate the mechanical behaviour of the fibre and the tows. This will complicate the parameters tuning procedure, as more data needs to be collected.

8.2 Fibre rotation effect

The last part of the stress strain curve is very different from the expected behaviour, in which fibres continue to hold weight until all of them fail. A possible reason can be due to the absence of the modelling of the fibre rotation due to the deformation of the elements.

As seen in [18], a study has been made regarding different failure mechanisms in ±45° unidirectional composites. Theoretical damage models were fitted to an empirical shear stress-strain curve, to represent the real failure behaviour; once this was done, a comparison has been made between the full model and the one without fibre rotation. For ±45° composites, the following formula is used for the estimation of the rotation angle:

$$\Delta\vartheta = \tan^{-1}\frac{(1+\varepsilon_{xx})}{(1+\varepsilon_{yy})} - 45° \quad (53)$$

Where ε_{xx} and ε_{yy} are the tow deformations in the load and lateral directions, respectively. By applying this formula to the simulation results of the RVE's, rotations up to 2.67° were measured at the final imposed displacement. Assuming that a tow element does not fail over the course of the simulation, his elastic properties can be estimated as:

$$E_1 = E_{xx}\sin\vartheta + E_{yy}\cos\vartheta$$

Where E_{xx} and E_{yy} are the Young's moduli in the longitudinal and lateral directions, and theta is the orientation angle. If the value of 2.67° of angle variation is assumed, the variation between initial and final elastic moduli is 3.87%. This value of maximum error leads us to conclude that, in this case, fibre rotation is not important.

To confirm this statement, the same formulation has been applied to the data available from the DIC of the tensile test. To have accurate results, the input deformations in the formula must be from fibre rich zones, while the available data is averaged over all the material. As the matrix deformation is usually greater than fibre one, the deformations and subsequent calculated angle will be overestimated. The empirically estimated final rotation angle is equal to 3°, slightly higher than the simulated one, as expected. Still, this confirms the negligeable effect of fibre rotation.

8.3 Statistical considerations

To fully comprehend the differences between RVEs, some statistical considerations can be made on the results. If the mean value is representative of the global behaviour, the standard deviations describes the variability inside the specimen. In this case, the

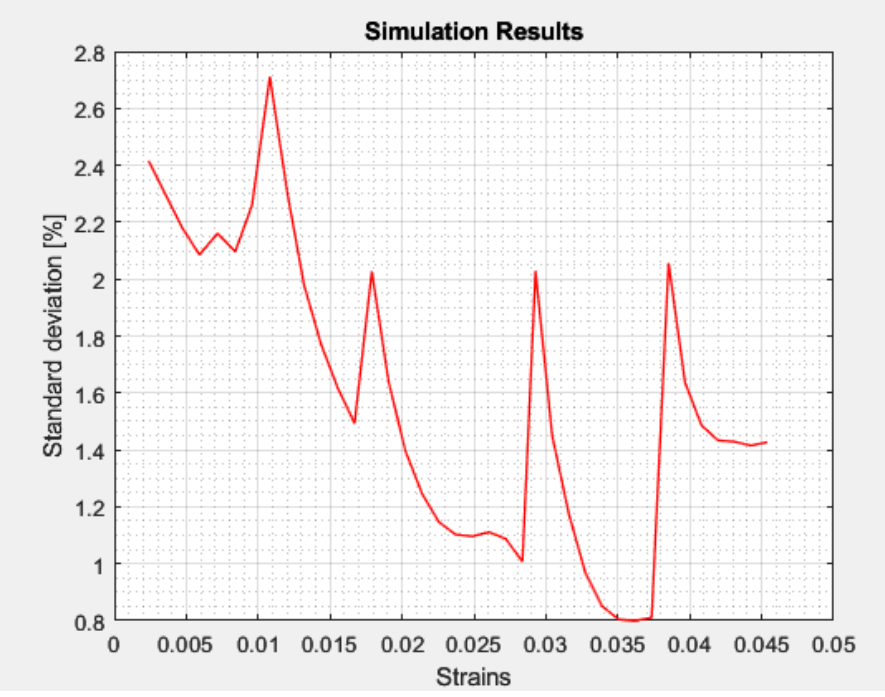

Figure 26 - Standard deviation between stresses values along the mean strains

standard deviation has been computed between all the stress values at each simulation step, as a percentage value of the mean stresses (Figure 26).

It can be seen that the general trend is descending, which is expected as the mean stress value typically increases with the steps. The trend is quite discontinuous, as there are spikes in the values. This can be attributed to the numerical fluctuations due to the type of convergence norm used. In the end, the values do not exceed 2.8%. This could be due to the fact that the sampled specimen is quite small compared to the RVE size, and some defects have been simulated more than once.

8.4 Comparison with the ideal RVE

As regards the perfect RVE, the damage mechanism is the same, and its damage variables behave in the same way.

The difference lays in the elastic modulus, ultimate strength, and the damage onset, which appears slightly later. This coincides with the expected behaviour, as the real material contains voids and other imperfections.

A comparison can be done on the effect of the voids in the mechanical properties of the material, especially Young's modulus and ultimate stress.

	Perfect model	*Mean real model*	*Difference [%]*
Elastic modulus [MPa]	6525	6024	7,7
Maximum strength [MPa]	63,6	59,3	6,7

Table 6 – Comparison between mean real and perfect model

a)

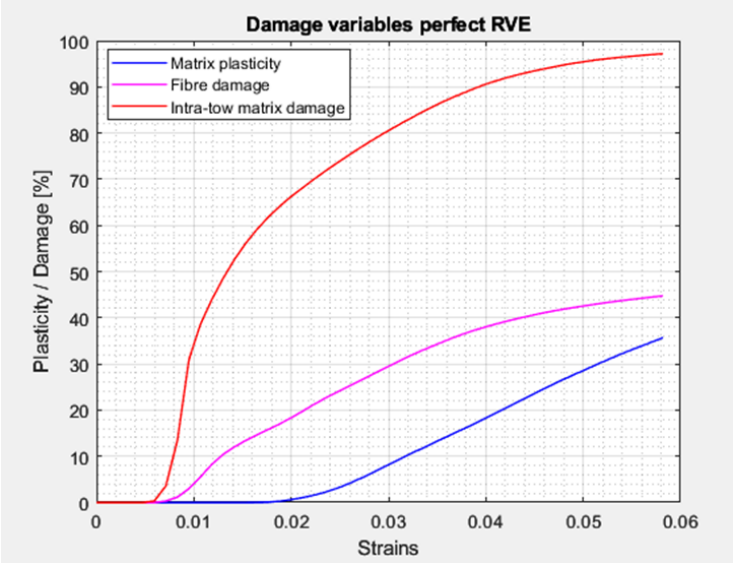

b)

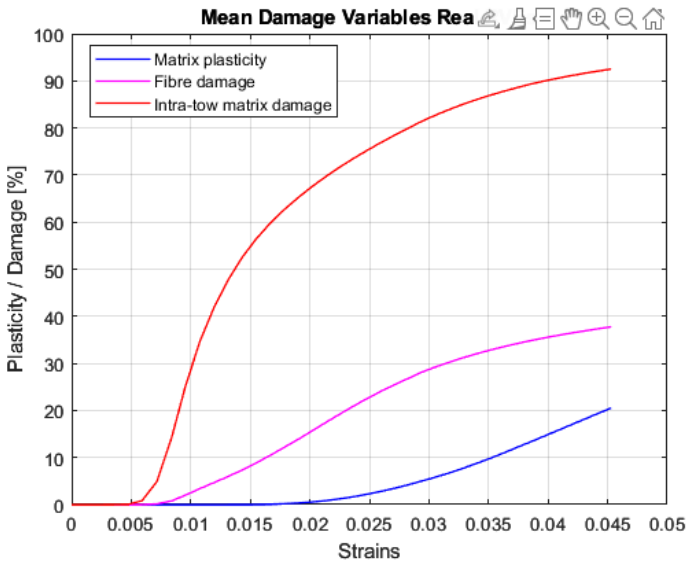

Figure 27 - Damage variables of the perfect (a) and mean real (b) RVEs

8.5 Void analysis

As demonstrated with the simulations, the effect of voids and other defects on the mechanical properties is significant, as the reduction in ultimate stress and elastic modulus is up to 7%. Let's now analyse the characteristics of voids in the extracted RVEs, starting from the volume fraction.

Table 7 – Results from each simulated RVE, in order of extraction

RVE n°	Volume fraction [%]	Young's modulus [MPa]	Maximum Stress [MPa]
1	1	6141	60
2	1.956	5846.7	58.2
3	1.083	6194.5	60.5
4	1.236	5917	58.5
5	1.25	6021	59.3
6	2.427	5923.3	58.6
7	1.247	5997.5	59.5

Table 8 – Results from each simulated RVE, in order of volume fraction

RVE n°	Volume fraction [%]	Young's modulus [MPa]	Maximum Stress [MPa]
1	1	6141	60
3	1.083	6194.5	60.5
4	1.236	5917	58.5

7	1.247	5997.5	59.5
5	1.25	6021	59.3
2	1.956	5846.7	58.2
6	2.427	5923.3	58.6

The average volume fraction of the real specimen is 1.457, with a standard deviation of 0.5283, which is equal to 36,26% of the mean. This value demonstrates the high scatter in volume fraction inside a specimen and strengthens the idea of a statistical representation of the void effect.

As anticipated, the void volume fraction is not the only important variable but also shape and size are of interest. It can bee seen especially from Figure 28 that there are mainly two types of voids: microvoids, which are the ones that are scattered inside the RVEs and are made up of few voxels, and large macrovoids trapped between layers, with their main plane parallel to the lay-up direction. The difference in size is significant; known that the single voxel has a side length of 0.1 mm, some microvoids are made up of only one voxel, as other macrovoids have lengths on the order of magnitudes of the millimetre. All the voids from the simulated RVEs have been represented in Figures 29-35.

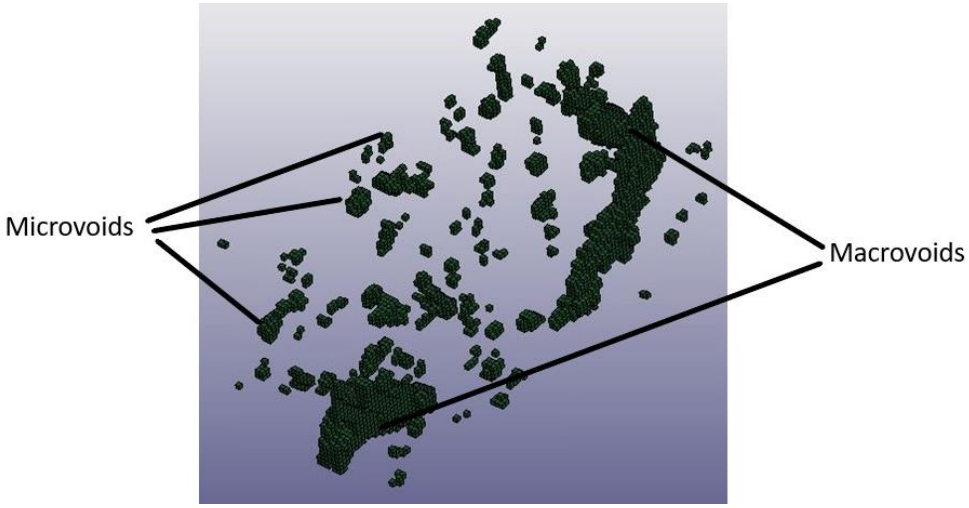

Figure 28 – Examples of micro and macro voids from the 2nd RVE

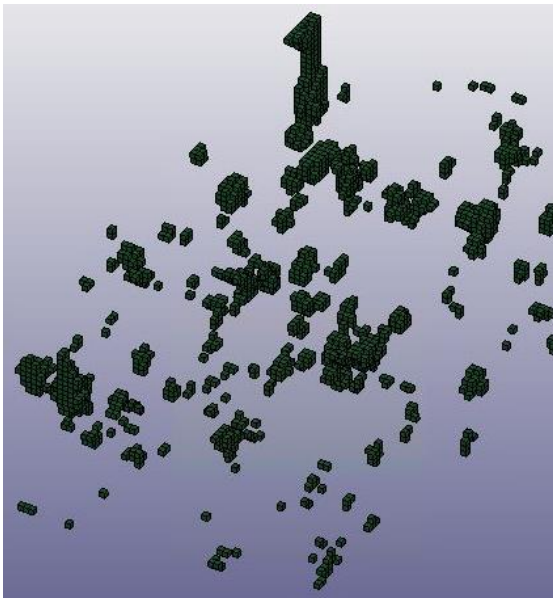

Figure 29 - Voids from 1st RVE

Figure 30 - Voids from 2nd RVE

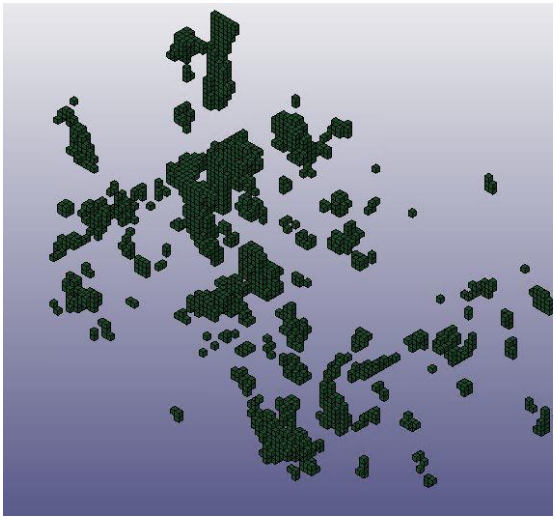

Figure 31 - Voids from 3rd RVE

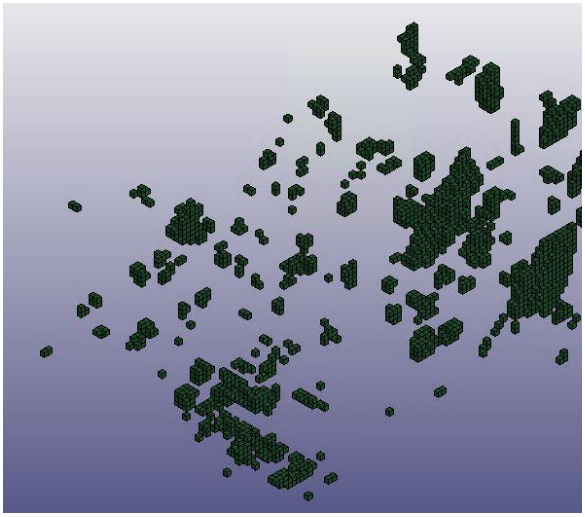

Figure 32 - Voids from 4th RVE

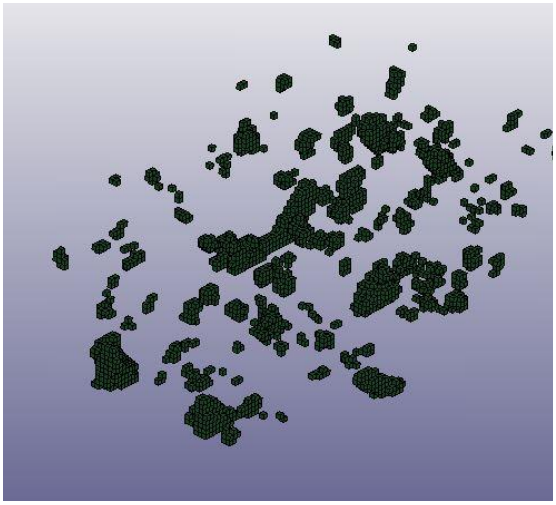

Figure 33 - Voids from 5th RVE

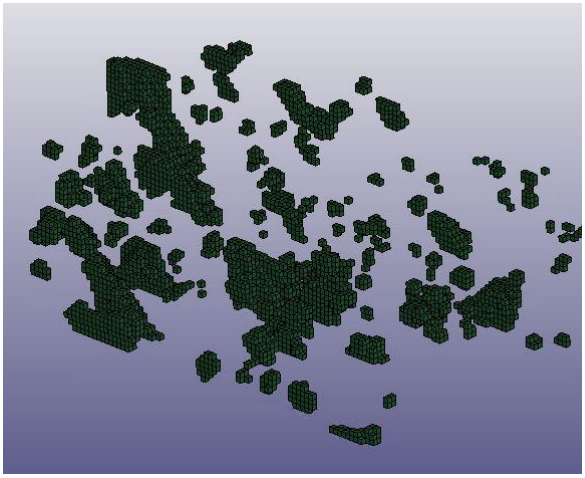

Figure 34 - Voids from 6th RVE

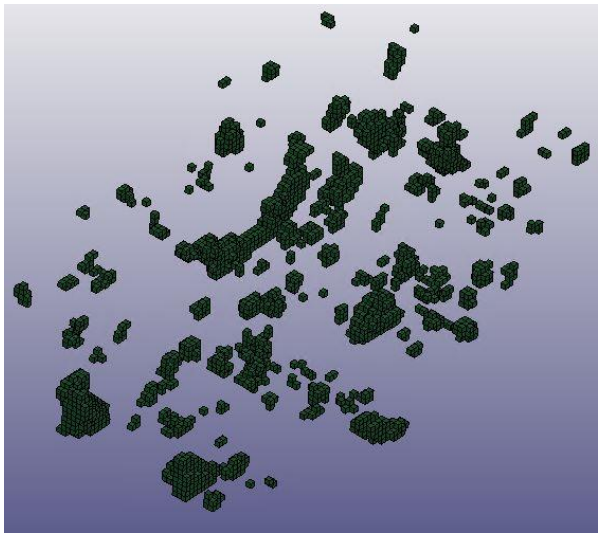

Figure 35 - Voids from 7th RVE

Some voids have been extracted more than once, totally or partially. This can be expected from the random extraction process, and the number of RVE chosen.

A clear example of the stress intensification process can be seen on the RVE n°3. Focusing on the void in Figure 36:

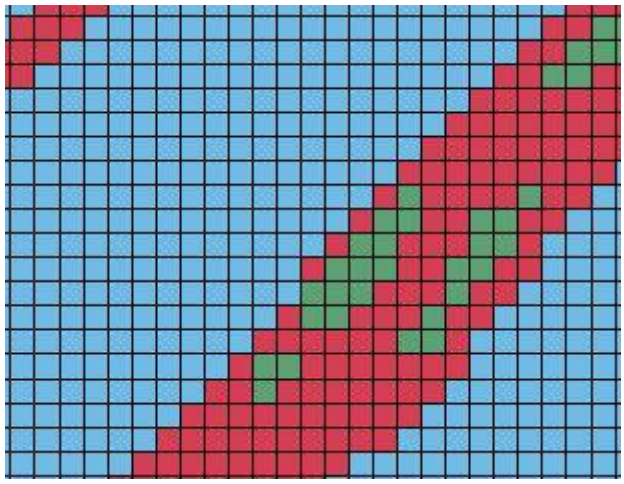

Figure 36 - Example of void from the third RVE

The tows are highlighted in blue, the voids in green, and the matrix in red. When the displacement is applied, the tow near the void starts to be subjected to higher stresses than the bundle element that are farther. In the Figure 37, Von Mises equivalent stresses are shown in a colour scale, as an index for stress intensification phenomena. The red indicates the highest stress, while the blue the lowest. The bundle near the voids, shown in red, are subjected to equivalent stresses up to 190 MPa, while the furthest tow elements (in yellow) reach values up to 132 MPa. The notch factor is equal, in this case, to 1.44. As seen Figure 38, this notch effect leads to premature failure of the fibres. The colour scale shows the Von Mises stresses, and as it can be seen, some tow elements have turned blue. This means that their stress has been brought to zero because they have

failed. In this case, the intra-tow damage has already started also far from the voids, but in their vicinity is more advanced.

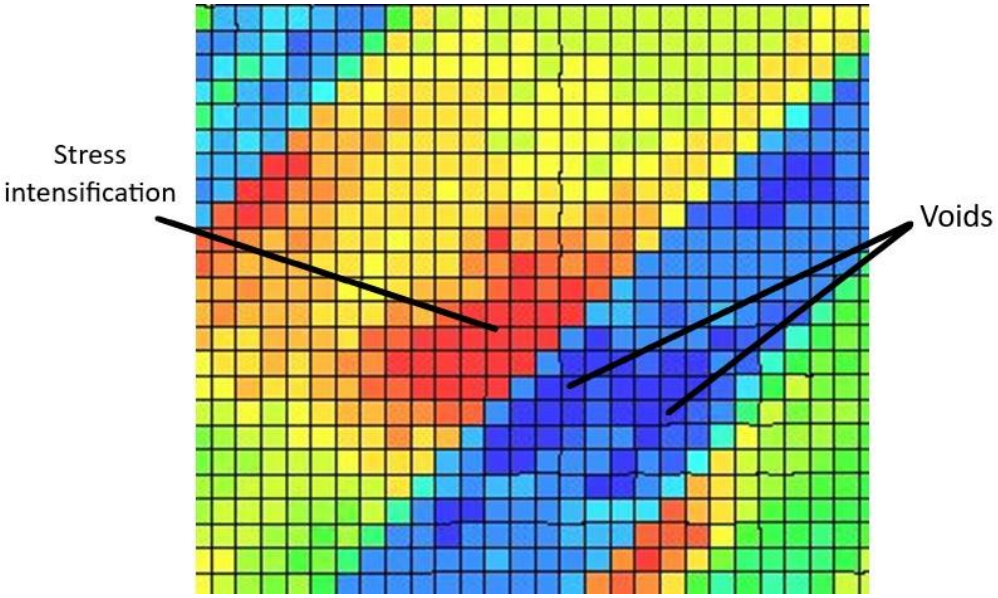

Figure 37 - Stress intensification phenomenon

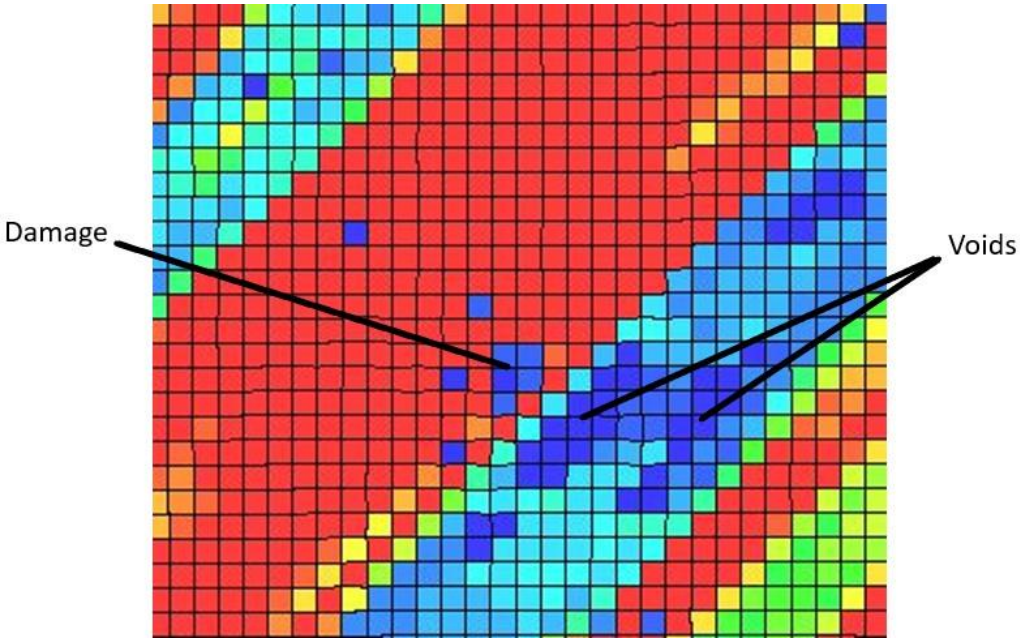

Figure 38 - Damage initiation due to the notch effect of the voids

The stress concentration effect does not affect only the tows, but also the matrix. Another comparison can be done on the RVE n°6, which has the highest volume fraction of voids.

In Figure 39b the colour scale shows the Von Mises equivalent stresses. The red colour indicates a stress value of 76.4 MPa, while the farther matrix element in green-yellow hold a value of 47.1. In this case, the stress intensification factor is equal to 1.62. The effect gets even greater towards the end of the simulation, as it can be seen on Figure 39c. There, damage values of the matrix are represented. If the damage value is zero, the element did not reach the maximum stress, while a value greater than zero indicates that the maximum material stress has been reached and the distance from it. It can be seen

that in the same zone, maximum damage values of 0.91 are reached, while other elements remain undamaged

a) b) c)

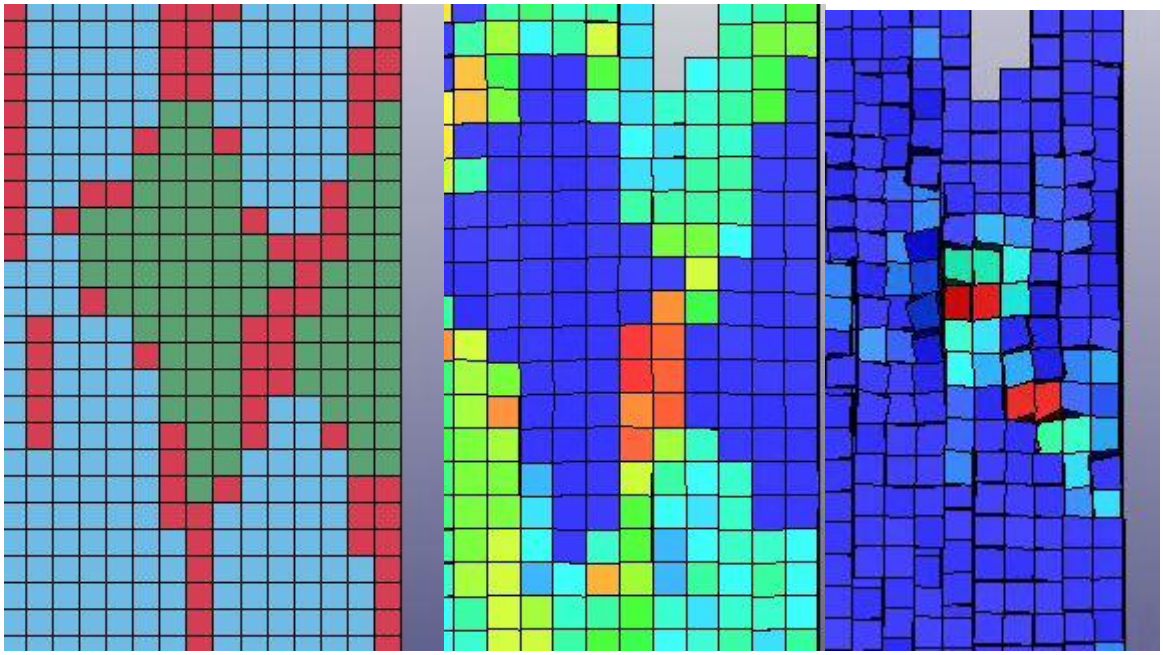

Figure 39 - Close up of the focus zone on the 6th RVE (a). Stress intensification phenomenon between voids (b). Damage variables around the voids (c)

Even if the number of RVEs is small to get to conclusive results, some evaluations can be made on the effect of void shape, size, amount and location, on the different RVEs, by looking at each stress-strain curve in Figure 40.

It can be seen that the highest values of stresses are present in the RVEs n°1 and n°3. These are the one with the lowest porosity, which is distributed among a large number of microvoids, with some bigger clusters. On the other hand, the lowest strength is observed in the 2nd and 4th RVEs. The 2nd one has a high void volume fraction compared to the mean value, and two macrovoids are present, so a higher detrimental effect is expected. On the other hand, the 4th RVE does not have a high void volume fraction neither big clusters. In this case, the detrimental effect can be due to the closeness of the voids to critical zones. The 6th RVE has the highest void volume fraction, and a noticeable presence of macrovoids. Its curve also displays an unusual dip in stress, only near the peak, while in the elastic part its behaviour is close to other RVEs. In this case, the presence of the dip could lead to conclude that it is caused by the void's presence, but that is not necessarily true, as it could be due to the premature convergence phenomenon explained earlier. A simulation with a stricter norm should be run to make definitive statement.

The trend appears to be coherent with the literature. While low void fraction with small dimensions lead to better performance, and macrovoids, critical placement, high porosity has a detrimental effect, it is unclear how these effect influence combines. For example, an RVE with porosity, smaller voids, but critical positioning of the defects can yield lower

performance than a high porosity, big voids, with not-so-critical positioning. That is the case for the 6th and 4th RVEs, respectively.

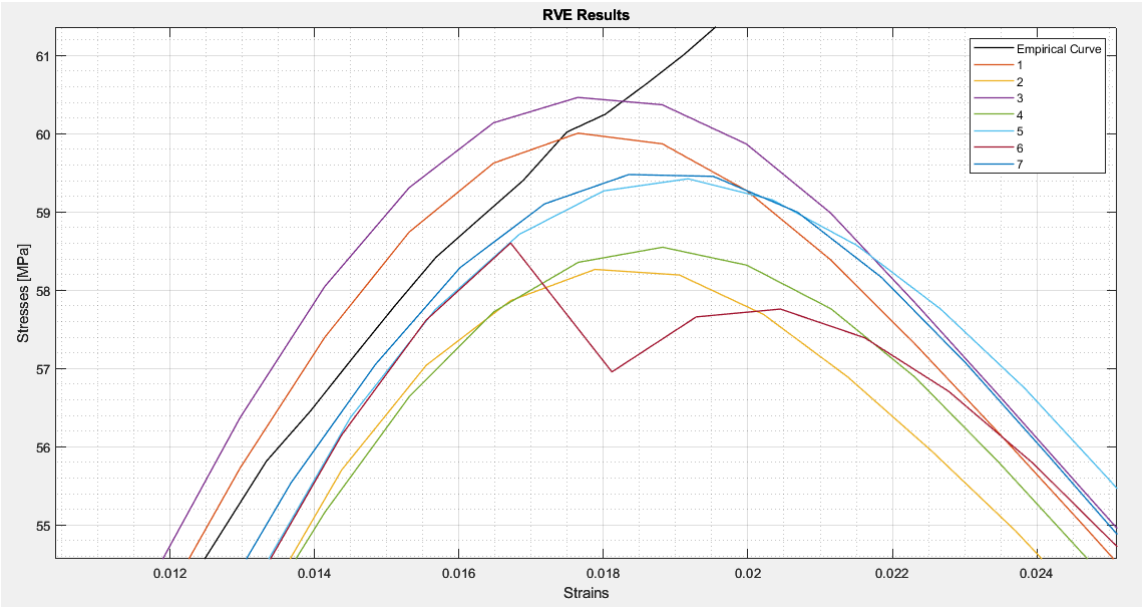

Figure 40 - Close up of the stress strain curves of all the RVEs

9 Conclusions

Considerations on the proposed procedure have to be made from two different aspects: convenience and coherence. Convenience focuses on how the procedure is done, to evaluate if it is simpler, faster, and cheaper to run than other methods, and so if it is convenient to use over other available choices. Coherence focuses on the quality of the results, their correctness, and the usefulness.

9.1 Convenience

From the start of the development of the procedure, a focus has been always maintained in the simplicity and quickness. The main objectives that have been reached are:

- Material properties have been estimated by general purpose data, avoiding costly experimental campaigns on the constituents properties study. A simple tensile test on a specimen of the final material has been used, reducing the empirical investigation to the simplest test case.
- Basic-intermediate Matlab™ code has been used for preparation, automatization, and post processing of the results. Some codes were already available at the department, but other codes were developed or downloaded from the internet. For example, the meshing phase has been done by re-adapting downloaded code from Matlab™ exchange online platform, and use of complex and expensive softwares like Altair Hypermesh™ has been avoided.
- Basic Ls-Dyna™ material cards have been used, so that the programming of a user defined subroutine is not necessary. This procedure would be tedious and time consuming.
- The simulation time has been shortened to a mean of 1 hour and 55 minutes per RVE, which is a very good result. The computational power needed is not too large, as institution like universities, research groups, and companies commonly have such servers.
- Once the parameters have been set, the simulation preparation has been almost entirely automatized. Only the fibre orientation input has been done by hand for better precision, but it can be automatized. The uses must only run two Matlab™ scripts, copy and paste ".k" and ".txt" files, other than few corrections and modifications to them. This procedure did not take more than 15 minutes and can be done while other simulations run.

In the end, it can be said that a good result has been achieved in terms of velocity and ease of use, and from this point of view the procedure is very convenient.

9.2 Coherence

The final results of the simulation give a good estimate of the failure mechanisms of the material. By doing simple assumption on the post-failure behaviour of tows, and using theorical formulation, a good fit between the expected failure and stress-strain behaviour has been obtained. Despite this, some limitations have been encountered in this study:

- The unrealistic notch effect of the matrix around fibres, which is due to element discretization and material properties in a specific boundary zone. This did not allow to correctly interpolate the real and simulated results, at least in this case. It can be said that the fracture in 45° unidirectional composite is a complex phenomenon, and leads to the highest strain to failure, compared to other angled ply. The error appears at quite high strains, so it could not be present for simpler load cases, or differently oriented plies. A possible solution is to insert an intermediate zone between tows and matrix, whom properties are calculated with the same rule of mixtures used for the tows, but a lower fibre volume fraction, and a more ductile behaviour.
- There is not a lot of information around the beta factor in literature. It is simply stated that it can be changed in a case-to-case basis, to interpolate empirical results. But, as in this case it is necessary to predict real values from a simulation, it would be convenient to know if beta is a property of the material, and only depends on decohesion, debonding, and other failure modes inside the tows, or its value must change for each load case. This could be simply investigated by studying other load cases and experimentally validating the results.

Other than these limitations, considerable results have been reached in the prediction and monitoring of the failure mechanisms:

- The development of three failure indices, which help to understand the global behaviour of the material. They can be calculated directly from the results, without complex computational post processing, but only with the same homogenization procedure already put in place for the stresses and strains. These indices agree with the failure mechanisms observed in the real specimen.
- The possibility to evaluate the effect of voids in mechanical properties. This can be done not only on a statistical approach, looking at the global responses and stochastic analysis, but also on a deterministic level, by looking at the specific void, in a specific location, of a specific size.
- An estimate of the fibre rotation effect, which is usually negligeable, but in very particular cases it can affect the final results.
- The RVE shape effect on the final results: in some cases, like this one, cubic RVE gave different results than the rectangular one. This can influence the choice of examined RVE, which is done usually by an estimation on the convergence of the elastic properties: despite the fact that they were the same, the failure behaviour showed differences, due to the tow geometry.

In conclusion, the procedure holds interesting results, especially for its speed and simplicity, once the main optimal parameters of the simulation are found. Further improvements and investigation have to be done to reduce computational errors and validate the results for different materials and different load cases.

References

[1]: Voids in fibre-reinforced polymer composites: A review on their formation, characteristics, and effects on mechanical performance. Mahoor Mehdikhani, Larissa Gorbatikh, Ignaas Verpoest, and Stepan V. Lomov.

[2]: The effect of voids on matrix cracking in composite laminates as revealed by combined computations at the micro- and meso-scales. Mahoor Mehdikhani, Nikolay A. Petrov, Ilya Straumit, António R. Melro, Stepan V. Lomov, Larissa Gorbatikh.

[3]: Mesoscale analysis of damage growth in woven composites. Aurélien Doitrand, Christian Fagiano, François Hild, Vincent Chiaruttini, Anne Mavel, Martin Hirsekorn.

[4]: Mesoscopic and multiscale modelling in materials. Jacob Fish, Gregory J. Wagner and Sinan Keten.

[5]: Data driven statistical method for the multiscale characterization and modelling of fibre reinforced composites. A. Ciampaglia.

[6]: Input data for test cases used in benchmarking triaxial failure theories of composites, A.S. Kaddour, M.J Hinton.

[7]: A single element test. John Robinson.

[8]: Failure criteria of unidirectional carbon fibre reinforced polymer composites informed by a computational micromechanics model. Qingping Sun, Guowei Zhou, Zhaoxu Meng, Haiding Guo, Zhangxing Chen, Haolong Liu, Hongtae Kang, Sinan Keten, Xuming Su.

[9]: LS-DYNA Theory Manual, volumes I, II and III. Livermore Software Technology Corporation (LSTC), Livermore.

[10]: Review of solid element formulations in LS Dyna, properties, limits, advantages, disadvantages. Ls Dyna forum 2011, Tobias Erhart.

[11]: Texgen™ user guide. https://texgen.sourceforge.io/index.php/User_Guide .

[12]: Consistent application of periodic boundary conditions in implicit and explicit finite element simulations of damage in composites. D. Garoz, F.A. Gilabert, R.D.B. Sevenois, S.W.F. Spronk, W. Van Paepegem.

[13]: Jiexian Ma (2024). voxelMesh (voxel-based mesh) https://www.mathworks.com/matlabcentral/fileexchange/104720-voxelmesh-voxel-based-mesh , MATLAB Central File Exchange.

[14]: Pseudo-ductile effects in ±45◦ angle-ply CFRP laminates under uniaxial loading: Compression and cyclic tensile test. M.C. Serna Moreno, S. Horta Muñoz.

[15]: Investigation of the ductile deformation potential of microscale epoxy materials. Janina Mittelhaus, Phil Röttger, Eduard Schill, Julius Jacobs, Bodo Fiedler.

[16]: Input data for composite material cards in Ls-Dyna™. https://dyna-composites.netlify.app

[17]: Simulating Laminated Composite Materials Using LS-DYNA Material Model MAT54: Single-Element Investigation. Paolo Feraboli, Bonie Wade.

[18]: Damage evolution in [±45]s laminates with fibre rotation. Carl T. Herakovich, Robert D. Schroedter, Alain Gasser, Laurent Guitard.

[19]: Quasi-static and dynamic response of cardanol bio-based epoxy resins: effect of different bio-contents. Andrea Iadarola, Pietro Di Matteo, Raffaele Ciardiello, Francesco Gazza, Vito Guido Lambertini, Valentina Brunella, Davide Salvatore Paolino.

Appendix A: Ls-Dyna™ and Abaqus™ comparison

On the first phases of the work, the choice of the finite element software fell on *Abaqus*™. This software, produced by *Dassault Systemes*™, is commonly used for these types of applications. This allowed to gain some confidence with both softwares and make some comparisons between them.

Abaqus is most common for FEM simulation, mainly because is more user-friendly. The interface is quite similar to the *Solidworks*™ one, as they are both manufactured by the same company. On the other hand, *LS-Dyna*™ is a much more powerful tool, as it has more material cards, a faster solver, and faster matrix-building phase.

Both softwares run on the keyword system. The *Abaqus*™ interface allows the unexperienced user to avoid having to cope with this system, which can be complicated. However, for some cases it is impossible to avoid, for example to import meshes and user-defined boundary conditions.

On the other hand, *LSPre-Post*™ does not hide this mechanic, but ease the work of the user by providing information for each keyword and parameter, automatic syntax, and visual representation of the geometries. This shared system allows compatibility between software allows the transition between them, as *Abaqus*™ input files can be read by *LSPre-Post*™.

Abaqus™ has both implicit nonlinear solver and explicit solvers, but there are many differences from *LS-Dyna*™. Other than the lower amount of material cards, only simpler material models can be run with the implicit solver: for example, damage evolution in an elastic-plastic model is available only with *Abaqus*™*/Explicit* version.

Another example which closely regards the RVE simulation is the presence of only one failure criteria for composite models, which was Hashin's one. This model needed the specification of damage energy and could be run only on explicit. But the main inconvenience was that this material was available only for thick shell elements.

Thick shell elements are geometrically identical with solids, both having 8 nodes, but the difference stands on the treatment of local directions. As thick shell elements are designed for cases where the main two dimensions are greater than the thickness, stresses and strains are calculated only at the median plane in the third direction. This approximation is not very problematic for the RVE, as the composite has been subjected only to a biaxial strain state, but could be unacceptable if through-thickness properties need to be studied.

On the opposite, *LS-Dyna*™ has a wide choice of material cards; for composite materials, the cards 022, 054-055, 058, 059, 161, 162, 261 and 262 are available.

The main problem with *Abaqus*™ happened with the implementation of the periodic boundary conditions in explicit analysis. At first, the solver does not allow for unreferenced and unconstrained nodes. Then, once the dummy nodes are constrained or referenced to an element, the solver was not able to efficiently get to a solution. The

matrix building phase ended in 2 hours, but the, even after 15 hours, the solver was not able to write a single step. This was the main reason why the transfer took place.

Abaqus™ is still a valid tool for introduction to FEM simulations, and for general purposes which do not require high computational power. On the other hand, *LS-Dyna*™ is more suitable for advanced users and niche applications.

Appendix B: Methodology for fitting an empirical stress strain curve in Ls-Dyna Mat 024 and 081

Material cards 024 and 081 are commonly used to model elastic-plastic materials, especially steel, aluminium, and plastics. Hence, a method to quickly fit experimental stress-strain curves with the material card behaviour is useful.

At first, it is needed to understand how the card works.

Once the basic data like elastic modulus, Poisson's ratio and density are specified, the plasticity data must be given. To find the stress strain law of the material, the card adds the plastic strain to the elastic one, at each level of stress. The plasticity curve can be modelled in three ways:

- If the precise evolution of the plasticity is not of interest, the tangent modulus and yield stress can be specified. This will lead to a bilinear stress strain evolution.
- If the plasticity curve contains less than eight points, the definition of a load curve with the *DEFINE_CURVE option can be skipped, and data can be given directly in the card, as ES and EPS values.
- If more data is needed, a curve must be defined and referenced with the LCSS option.

The points of the plasticity curve must be defined as effective plastic strain versus stress. These can be calculated with the following procedure:

- With the help of MATLAB™, plot the empirical curve and the elastic modulus line. This can be done by plotting the real strains against the product between such strains and Young's modulus.
- Use the elastic modulus as a reference. Choose a certain value of yielding, depending on a case-to-case basis. Then, at certain levels of stress, calculate the difference in strain between the real curve and the Young's modulus. That is the effective plastic strain of the card.

The number of points depends on the level of precision of interest.

For the material card 024, the failure is specified as effective plastic strain in the FAIL box. This is the value of plasticity at failure. When an element with this material model exceeds the FAIL value in an implicit analysis, the stresses are not reduced to zero instantaneously, but over a certain amount of strain. The length of this controlled decrease appears to depend on the slope of the line that goes through the last two points specified in the plasticity curve. This behaviour has to be taken in consideration, as it can lead to an unwanted pseudo-damage evolution. That is not the case in explicit analyses, where the element is abruptly deleted from the simulation.

If damage evolution is needed, the card 081 must be used. The modelling of the plasticity is the same, and differences start after the peak plastic strain value is specified. This parameter is called EPPF in the card 081.

In Ls-Dyna, damage is intended as:

$$D = 1 - \frac{\Delta E}{E_0} \qquad (B1)$$

where ΔE is the variation in elastic modulus, and E_0 is the pristine initial modulus.

There are two ways to model damage: if the evolution over strain is not of interest, a value of EPPFR can be specified. This will lead to a default linear damage evolution, where damage equals zero at EPPF and equals one at EPPFR. Linear damage means that the damage variable D will evolve linearly, not the stress-strain curve, which will follow a quadratic law.

If a precise damage evolution is needed, a curve linking the damage variable with effective plastic strain can be specified with the LCDM option. The curve can be defined with the following steps:

- Plot the curve obtained by the one element test with the card 024, but without failure. The card will interpolate plastic strains after failure based on the slope of the line between the last two points specified in the plasticity curve.
- Calculate the effective plastic strain after maximum stress as the difference between the strain of the one element test result and the elastic modulus curve.
- Correlate to each plastic strain value chosen a damage value. The damage is calculated as previously. The elastic modulus variation is the difference between the original modulus, and the ratio between stress and strain of the empirical curve, at the chosen point.

As before, the choice of the number of points is up to the user.

It has been observed that, if the starting point of the damage curves coincides with the EPPF value of plastic strain, with a zero value of damage, a discontinuity can appear at the maximum stress. This could be due to problems between the interpolation of the end of the plastic curve and the beginning of the damage one. A solution is to impose a nonzero damage, with a value around 0.05-0.07.

	TITLE							
	Matrix 081							
1	MID	RO	E	PR	SIGY	ETAN	EPPF	TDEL
	300	1.550e-06	3000.0000	0.3500000	25.000000	0.0	0.0243400	0.0
2	C	P	LCSS	LCSR	EPPFR	VP	LCDM	NUMINT
	0.0	0.0	2	0	0.0	0.0	300	0
3	EPS1	EPS2	EPS3	EPS4	EPS5	EPS6	EPS7	EPS8
	0.0	0.0	0.0	0.0	0.0	0.0	0.0	0.0
4	ES1	ES2	ES3	ES4	ES5	ES6	ES7	ES8
	0.0	0.0	0.0	0.0	0.0	0.0	0.0	0.0

Figure B1 – material card 081_PLASTICITY_WITH_DAMAGE example values

A last consideration has to be done on the final failure. The card does not allow to cancel the element before damage reaches one. This can lead to numerical problems in implicit nonlinear simulations, due to the fact that with damage variables close to unity, the residual elasticity of the element is very low. This problem can be bypassed, by imposing a constant damage between 0.9 and 0.95 after failure. In this case, the element will have a very low residual elasticity and a small constant stress, which usually do not influence the solution, and do not trigger instability.

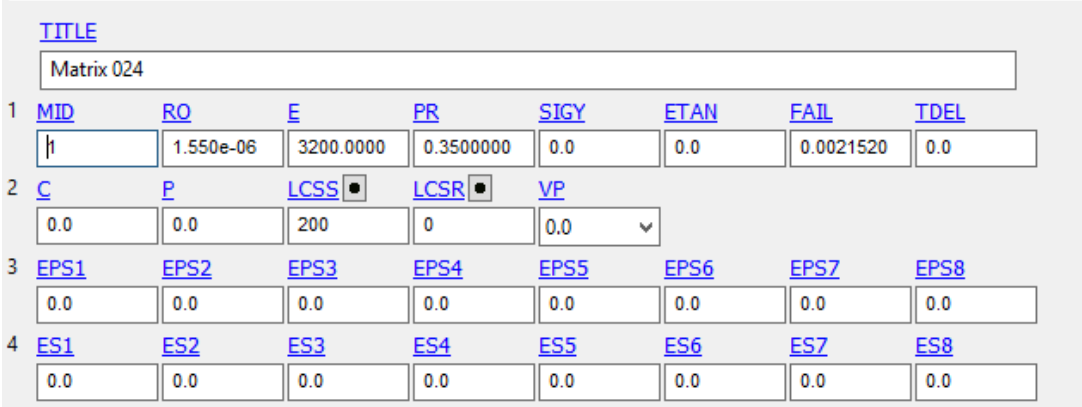

Figure B2 – material card 024_PIECEWISE_LINEAR_PLASTICITY example values